Journal of Medicinal Chemistry

Article

Rational Design Of Selective Adenine-Based Scaffolds For Inactivation Of Bacterial Histidine Kinases

Manibarsha Goswami, Kaelyn E Wilke, and Erin E. Carlson

J. Med. Chem., **Just Accepted Manuscript** • DOI: 10.1021/acs.jmedchem.7b01066 • Publication Date (Web): 21 Sep 2017

Just Accepted

ACS Publications

Journal of Medicinal Chemistry is published by the American Chemical Society. 1155 Sixteenth Street N.W., Washington, DC 20036

Rational Design of Selective Adenine-Based Scaffolds for Inactivation of Bacterial Histidine Kinases

Manibarsha Goswami,[1] Kaelyn E. Wilke[2] and Erin E. Carlson[1,2,3,4]*

[1] Department of Chemistry, University of Minnesota, 207 Pleasant St. SE, Minneapolis, MN, 55454, United States

[2] Department of Chemistry, Indiana University, 800 East Kirkwood Avenue, Bloomington, Indiana 47405, United States

[3] Department of Medicinal Chemistry, University of Minnesota

[4] Department of Biochemistry, Molecular Biology and Biophysics, University of Minnesota

Abstract

Bacterial histidine kinases (HKs) are quintessential regulatory enzymes found ubiquitously in bacteria. Apart from regulatory roles, they are also involved in the production of virulence factors and conferring resistance to various antibiotics in pathogenic microbes. We have previously reported compounds that inhibit multiple HKs by targeting the conserved catalytic and ATP-binding (CA) domain. Herein, we conduct a detailed structure-activity relationship assessment of adenine-based inhibitors using biochemical and docking methods. These studies have resulted to several observations. First, interaction of an inhibitor's amine group with the conserved, active-site Asp is essential for activity and likely dictates its orientation in the binding pocket. Second, a N-NH-N triad in the inhibitor scaffold is highly preferred for binding to conserved Gly:Asp:Asn residues. Lastly, hydrophobic, electron-withdrawing groups at several positions on the adenine core enhance potency. The selectivity of these inhibitors was tested against Heat Shock Protein 90 (HSP90), which possesses a similar ATP-binding fold. We found

that groups that target the ATP-lid portion of the catalytic domain, such as a six-membered ring, confer selectivity for HKs.

Introduction

The slow progress in the field of antibacterial drug discovery can be attributed to the lack of novel targets in bacteria, especially those that will be less susceptible to the evolution of antibiotic resistance. It is postulated that targeting bacterial virulence rather than viability could be a powerful new strategy.[1] Apart from preventing harmful bacteria from colonizing the host, antivirulence therapies have several advantages that have been recently highlighted.[2-4] Briefly, antivirulence agents will not kill bacteria but rather deactivate pathogenic mechanisms, resulting in less selective pressure for the evolution of resistant species.[5] Since these compounds are not bactericidal, they may preserve the natural host microbiome by fighting only pathogenic infections.[2, 6, 7] Significantly, this strategy increases the repository of antibacterial targets not yet explored with clinical implications of superior antimicrobials with new mechanisms of action.[3] It has been hypothesized that antivirulence therapies will be effective when used alone, in combination therapy with traditional antibiotics, or as a prophylactic treatment.[2, 3, 7]

Many virulence factors in both Gram-positive and Gram-negative bacteria are regulated by bacterial signaling, primarily through two-component systems (TCSs).[8] For example, in the pathogenic bacterium *Staphylococcus aureus*, the SaeRS TCS affects the production of over 20 virulence factors.[9] The PhoPR system controls polyketide-derived lipid biosynthesis in *Mycobacterium tuberculosis,* and its absence causes dramatic changes to colonial and cording morphology of this highly dangerous microbe.[10] In *Pseudomonas aeruginosa,* many TCSs, including PPrBA, are responsible for activating virulence genes, cell motility, and quorum

sensing signal production.[8] With growing evidence that TCSs are intimately involved in bacterial virulence, interest in the study of these ubiquitous systems has dramatically increased in recent years.[11-15]

TCSs are composed of homodimeric enzymes known as histidine kinases (HKs) and their cognate response regulators (RRs). Through TCSs, bacteria respond to many environmental stimuli, such as ions, temperature, pH, oxygen pressure, auto-inducers, and contact with host cells.[16] Once a signal is received, ATP binds to the catalytic and ATP-binding (CA) domain of HK and autophosphorylates at a catalytic histidine residue of the dimerization and histidine phosphotransfer (DHp) domain.[17] In a relay event, this phosphate group is transferred to a conserved aspartate on the RR, which then often binds to DNA to yield a downstream genetic response. In addition to virulence, TCSs and HKs have been associated with antibiotic resistance in many pathogenic strains, such as the VraS of *S. aureus* that is linked to vancomycin-[18] and daptomycin-resistance[19] and MtrAB of *M. tuberculosis*, that participates in efflux pump regulation of multidrug resistance (MDR) and survival inside macrophages.[8] Consequently, there has been great interest in discovering inhibitors of TCSs. Recently, Wells and Marina identified phenyl ring-based putative HK inhibitors using a combination of *in silico* and *in vitro* screens that have broad-spectrum antibacterial effects against both Gram-positive and Gram-negative pathogens.[20] In a similar approach, Meffre and coworkers designed thiophene derivatives as HK inhibitors and evaluated their potential as adjuvants for the treatment of resistant bacteria.[21]

We have also reported the discovery of HK inhibitors by the development of a fluorescence polarization (FP) assay to identify compounds that target the CA domain.[22] Highly conserved across HKs, it contains the Bergerat fold that is characteristic of the GHKL (Gyrase, Heat shock proteins, histidine Kinase, MutL) family but is absent in mammalian kinases.[23] We

envisioned that targeting this conserved domain would inactivate several HKs simultaneously for a broad-spectrum type antibiotic therapy. A high-throughput screen for inhibition of HK853 (*Thermotoga maritima*) resulted in 119 hits. Further analysis for dose-dependent activity against HK853, as well as VicK (*Streptococcus pneumoniae*) and CheA (*Escherichia coli*) yielded nine lead compounds capable of inhibiting multiple HKs.[22]

Four of the nine leads (and 19 of the original 119 hits) contained an adenine core scaffold, an expected result given that the target protein binds to adenine-nucleotides. The adenine chemotype is considered a "privileged scaffold"[24] as many natural product-derived or synthetic FDA-approved antiviral and anticancer drugs are purine-based and hence are likely to be more successful clinically. Interestingly, all of our adenine-based leads [6-*N,N*-dipropyl adenine (**1**), 6-*N,N*-morpholine adenine (**2**), 6-*N*-phenylethyladenine (**3**), 6-*N,N*-(3,3,5-trimethylcyclohexyl) adenine (**4**)] were functionalized at the 6-position on the ring with various secondary or tertiary amines (Figure 1a).[22] To better understand the structural requirements for inhibition of these proteins, we conducted structure-activity relationship (SAR) studies with complementary adenine analogs. In addition, given the importance of other ATP-binding proteins in eukaryotic biology, we sought to identify compounds that selectively target HKs over eukaryotic kinases (EKs) and other GHKL proteins (i.e., heat shock proteins).

Given the similarity of our leads to the natural substrate of the HKs, we sought to further examine the binding of ATP/ADP to the CA domain (Figure 1b,c,d). Previously, we conducted multiple sequence alignment of 150 HK homologs and generated a map of the highly conserved residues in the ATP-binding pocket.[25] The CA domain of HKs consists of a Bergerat fold (Figure 1d shows the conserved N-, G1-, G2-, G3-, F- boxes), which is unique to the GHKL family. By comparing three different HKs co-crystallized with nucleotides – HK853 (*T. maritima*) with

ADPβN (PDB:3DGE, Figure 1c),[17] WalK (*Bacillus subtilis*) with ATP (PDB:3SL2)[26] and PhoQ (*Escherichia coli*) with AMP-PNP (PDB:1ID0)[27] (Figure S1) – we observed many similarities (Figure 1b, S2). We also compared PDB:2C2A (Figure 1b), which is also the co-crystal of HK853 with ADP (in absence of its cognate partner RR468) along with the above structures as it has crystallographic information of the water molecules within the protein unlike PDB:3DGE. The direct ligand–protein interaction is a hydrogen bond (H-bond) between a deeply seated, conserved Asp (3DGE/2C2A D411, 3SL2 D533, 1ID0 D415) of the G1 box with the exocyclic amine of the adenine ring. The carbonyl group from the same Asp residue interacts with N1 through a H_2O molecule, which also binds to a conserved Gly (G1 box; 3DGE/2C2A G415, 3SL2 G537, 1ID0 G419). The highly conserved Asn from the N-box (3DGE/2C2A N380, 3SL2 N503, 1ID0 N389) acts a bridging residue that participates in an H_2O-mediated H-bond with N-7 on the adenine and ionic interactions with the β-phosphate and the co-factor Mg^{2+} ion (Figure 1b, S2). Apart from these hydrophilic interactions, the adenine ring sits between the hydrophobic residues Tyr (2C2A Y384, 3SL2 Y507, 1ID0 Y393), forming π-π stacking, Ile/Val (3DGE/2C2A I424, 3SL2 V546, 1ID0 I428), and Leu (3DGE/2C2A L446, 3SL2 L568, 1ID0 L446), which also make contacts to the α-phosphate. Finally, additional bonds that anchor the nucleotide are the coordination of the phosphates to the octahedral Mg^{2+} ion and to basic residues: Lys from the N-box (3DGE/2C2A K383, 3SL2 K506, 1ID0 K392) and Arg from the F-box (3DGE/2C2A R430, 3SL2 R552, 1ID0 R434). As the β- and γ-phosphates interact with the F-box on the ATP-lid, this flexible loop is responsible for presenting a favorable conformation for the phosphate transfer to the DHp domain. The interactions observed here are corroborated by similar analyses.[17, 26-28] In summary, several conserved residues interact in unison to tightly place ADP in the binding pocket, valuable insight that provides an opportunity to rationally design a potent and

competitive inhibitor to disrupt these interactions.

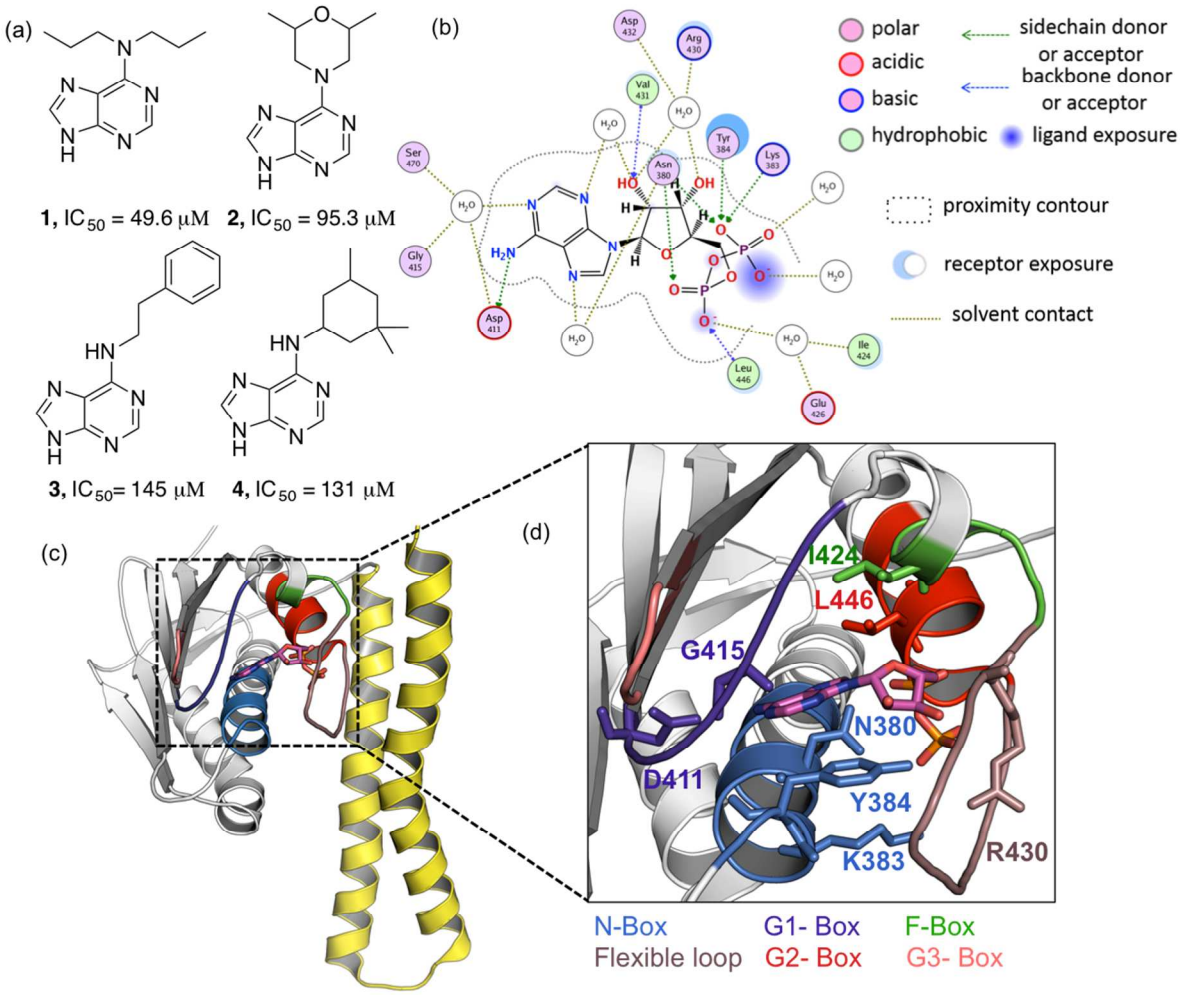

Figure 1. (a) Adenine leads with 6-C substitution from original screen. IC_{50} values are for HK853 inhibition, (b) Interactions of ligand obtained using MOE program[29] of HK853 co-crystallized with ADP (PDB:2C2A). The legend of interactions is also shown here, (c) Ribbon diagram of HK853 (PDB:3DGE) showing CA domain (white ribbon) and DHp domain (yellow ribbon), (d) Expansion of the CA domain showing features of the Bergerat fold and important residues binding to the co-crystallized ligand, ADP.

Results and Discussion

Assessment of ATP Binding Mode Through its Structural Elements

Most adenine-based drugs differ in the substituents on the scaffold and/or modifications that are intended to mimic the ribose and/or phosphates of ATP. Hence, we explored the SAR of adenine ring functionalization, as well as the key components of ATP to facilitate design of potent and selective HK inhibitors (Figure 2a). To test the importance of the α-, β-, and γ-phosphates, we measured the affinity of HK853 for ATP (**5**), ADP (**6**), and AMP (**7**)[22] using the activity-based fluorescence gel assay previously developed by our group (Figure 2b).[30] **5** and **6** had similar IC_{50} values (27 μM, 2.4 μM), whereas **7** had marginal activity (1030 μM), suggesting that one phosphate group is not enough for octahedral Mg^{2+} coordination or interactions with Arg on the ATP lid and Lys of the N-box for optimal binding.[26, 27] Indeed, when these residues are mutated in PhoQ (*E. coli*, K392A, R434A), a 50-fold loss in ATP-binding and catalysis was observed.[27] Next, we investigated the role of ribose in nucleotide–protein binding. In general, the solvent-exposed 22, 32-hydroxyls of the ribose unit interact with Arg and Val through a common H_2O molecule. We measured the ability of adenosine (**8**) to inhibit HK853 and found it to be moderately better than AMP with IC_{50}: 407 μM (Figure 2b, Table 1). This was surprising as the potency of the simple adenine base (**9**) (IC_{50}: 445 μM) is comparable to adenosine, which indicates that addition of the sugar does not increase affinity.

As mentioned, we were intrigued that the exocyclic N6 of most of the leads is not a primary amine as it is in the native substrate, but was instead decorated with hydrophobic substituents (Figure 1a). While the absence of 6-C-NH could preclude H-bonding with the conserved Asp or Gly, these N6-modified leads bound with greater affinity. These results prompted us to test the nucleoside/nucleotide analogs of some of the leads to decipher their impact on interactions with the active site. First, we examined HK853 inhibition by nucleoside

derivativeof lead **3,** 6-*N*-phenylethyladenosine (**10)** and observed that it had negligible activity despite the presence of the ribose moiety (Figure 2b, Table 1). Surprisingly, the related diphosphate nucleotide, 6-*N*-methylphenyl ADP (**11**) was only marginally better than **10** (Note: compound **11** has R = $PhCH_2$ was used instead of $PhCH_2CH_2$ due to commercial availability), indicating that presence of phosphates does not increase activity. To further evaluate the role of ribose, we tested the activity of 6-*N,N*-dipropyl adenosine (**12**), the nucleoside of lead **1** and similar to **10**. This analog failed to show any inhibition. Based on these observations and the likely disturbance of the critical and direct 6-NH bond to the conserved Asp, we speculate that compounds **1**–**4** bind to the CA domain in an orientation different from that of ATP/ADP in order to adopt other favorable interactions, exhibited by the lower IC_{50} values of these leads.

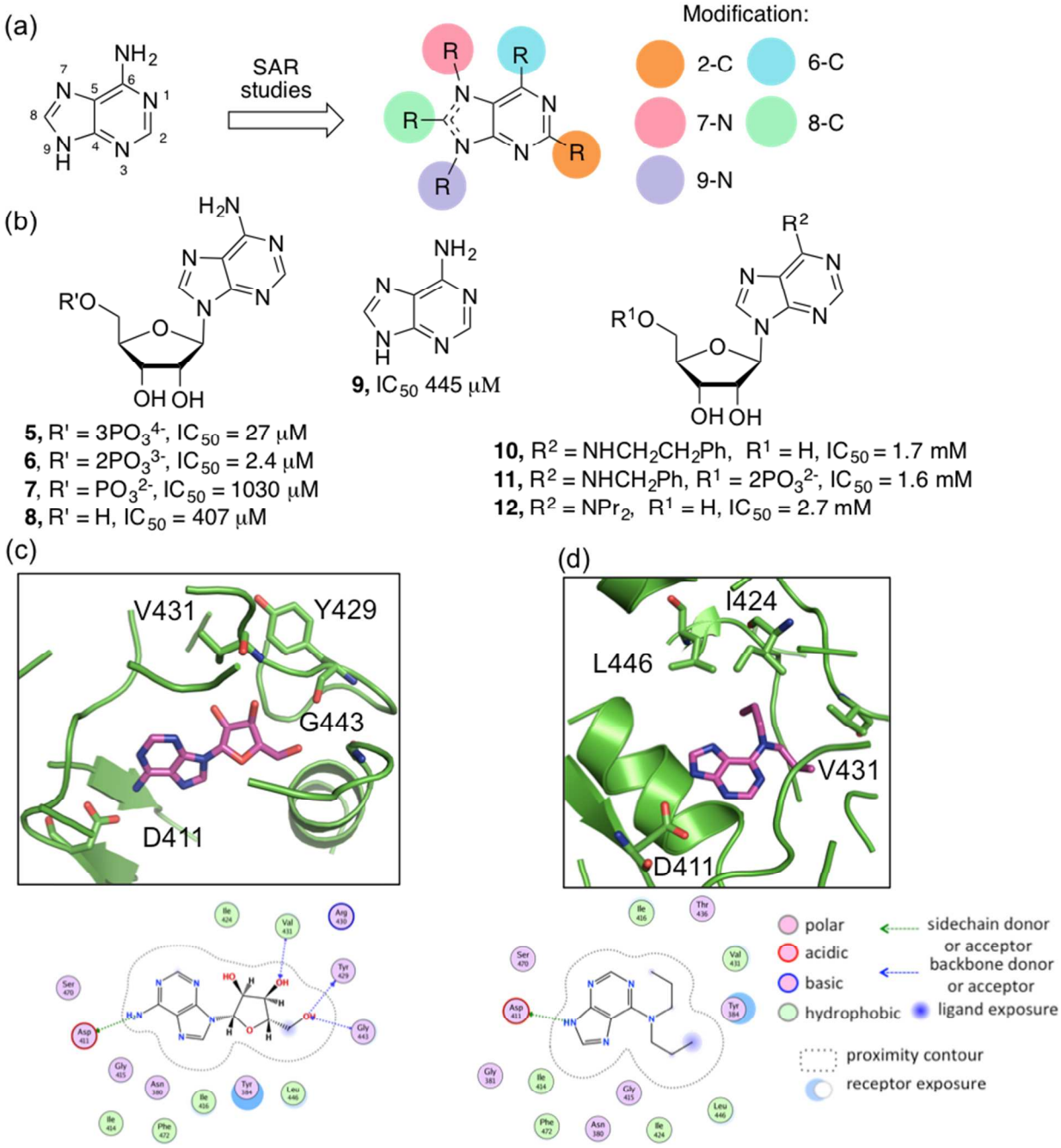

Figure 2. a) SAR approach to develop selective HK inhibitors. b) HK853 inhibitory activity of ATP and its components. Docking of **8** (c) and **1** (d). The top images show the docking pose of the compound in the receptor cavity. For clarity, only the cavity (green ribbons), and not the full protein, is shown, including important residues (sticks) for ligand-protein binding. The ligands

are shown as sticks with C = magenta, N = blue. These images were produced with PyMOL after docking was performed in SYBYL Surflex-Dock. The lower ligand–protein interactions were generated with MOE program. Legend of the possible ligand interactions generated by MOE.

To evaluate this hypothesis, we utilized molecular modeling to examine possible poses and interactions between the target protein and ligand. We used the Surflex-Dock Sybyl-X program to dock various ligands and MOE and PyMOL for computing interactions and visualizing. First, we docked **8** into the ATP-binding pocket of HK853 (PDB:3DGE) and found its binding poses to be similar to ADP-βN, the co-crystallized ligand (Figure 2c). This includes conserved interactions with D411 and ribose hydroxyl group interactions with V431 and G443 from the G1-box. A similar docking pose was observed with **9** (not shown). On the other hand, the docking of lead **1** yielded a binding pose different from that of **8** or **9** where its secondary amine 9-NH forms the crucial H-bond to the conserved Asp (Figure 2d). The propyl groups appear to access a nearby hydrophobic region consisting of conserved residues I424, L446 and V431. Our hypothesis that availability of the 9-NH for binding to D411 is essential for activity is consistent with the low potency of **12** (and compounds **10**, **11**), where the H-bond donor is no longer available due to the addition of the ribose. Similarly, the docking of lead **3** suggests that 9-NH H-bonds to D411 while the phenyl-ethyl group occupies the previously mentioned hydrophobic pocket (Figure S4a). In all of these compounds, another conserved hydrophobic region consisting of I411, I416 and F472 is situated near the adenine ring. Lead **3**'s riboside derivative **10** exhibited >20-fold decreased potency, further substantiating that 9-NH is important for lead binding, which is abolished when the ribose is present.

Contribution of the Conserved Aspartate Residue

As most of our hypotheses are based on the interactions of the conserved Asp with an H-

bond donor –NH, we compared the potency of these inhibitors between wild-type (WT) HK853 and the mutant protein HK853 D411N. Our previous competition assays were ineffective for detecting mutant HK activity and binding (BODIPY-ATPγS (Figure S3), ADP-BODIPY (Figure S3), respectively), presumably because both probes also require the D411 for binding. Thus to obtain data with the mutant protein, we utilized a thermal shift assay, differential scanning fluorimetry (DSF). DSF analysis has become popular in the past few years as it is a fast, robust, high-throughput method and can be easily performed with a commercially available dye on an RT-PCR instrument.[31, 32] DSF monitors the thermal unfolding of proteins in the presence of a fluorescent dye (SYPRO orange). When a ligand binds to a protein favorably, a shift (ΔT_m) is observed in the melting temperature of the protein (T_m) due to increased stability of the protein in the presence of the ligand. Using this strategy, we investigated if inhibitors bind to the HK in absence of the conserved D411. Thermal-shift assays or T_ms have not been reported elsewhere for HK853, a protein from the hyperthermophilic organism *T. maritima* and thus, expected to be very thermally stable.[33]

We first tested the T_m changes for the WT HK853 in the presence and absence of ADP **6**. We found that WT HK853 alone has a T_m = 70 °C, and in the presence of **6**, the T_m increases to 80 °C (Figure S6). A similar T_m shift is seen with lead **1**, which we expect binds to D411 through 9-NH. The ΔT_m of 10 °C shows that favorable binding occurs between **6** or **1** and the enzyme. The same experiment was executed with HK853 D411N (Figure S5). The D411N mutant protein has a T_m of 67 °C, which is lower than the WT T_m (Figure S6). In the presence of **6** or **1**, there was no significant change in the T_m value (≤ 2 °C), which suggests that D411 is crucial for interaction of **6** or the adenine inhibitors to the bacterial enzyme. Reduction of inhibitor affinity was seen by our group previously for guanidine-based compounds in mutant HK853 D411A.[25]

Inhibition loss was also seen by Zhao and coworkers in PhoQ (*Salmonella enterica*) when conserved D416 was mutated to alanine.[34] Apart from inhibitor binding, mutation of this Asp residue results in complete loss of kinase activity,[35] which further suggests the importance of D411 binding.

Evaluation of Additional Pyrimidine Substitutions

In addition to the 6-N and 9-N positions, we evaluated SAR for other positions on the adenine ring using a combination of commercially available and synthesized adenine/adenosine analogs. First, 2-aminoadenine (**13**) was tested for HK853 inhibition and surprisingly, it proved to be much worse (**13,** IC_{50} 2.6 mM) than **9** (Figure 3a, Table 1). Addition of a single $–NH_2$ group at the 2-C position resulted in 6-fold less potency, which suggests that this moiety might make the adenine electron rich, thereby weakening other non-covalent interactions. A similar trend was observed with aminoadenosine (**14**, IC_{50} 1.8 mM), which again suggested that ribose plays no role in effective binding and that the crucial H-bond to D411 is through 6-C-NH_2 and not 9-NH in these analogs (Figure 3a, Table 1). To investigate these hypotheses, 2-chloroadenine (**15**) and its riboside, 2-chloroadenosine (**16**) were tested as this group adds bulk on the 2-C position, yet is instead electron withdrawing. Interestingly, the chloro group enhanced potency of **8** and **9** by 10-fold. Similar to the chloro, the fluoro analogs, 2-fluoroadenine (**17**) and 2-fluoroadenosine (**18**) also exhibited superior potencies to **8**/**9** albeit to a lesser extent. Fluoro and chloro are both mildly deactivating groups and lower the pKa of the bases by at least 2.5 times.[36] A pKa decrease due to Cl may strengthen the H-bond of 6-C-NH_2 with D411, observed as increased affinity of the inhibitor. Increased affinity may also be influenced by: 1) the differences of the size of the group and/or its lipophilicity, or 2) the EWG –Cl favors the conserved π-π stacking of the adenine ring.[37] Nonetheless, further investigation was necessary,

particularly as to whether increased affinity is specific to –Cl or is common to other deactivating groups. Docking of **15** and **16** showed H-bonding between D411 and 6-C-NH_2, π-π stacking with Y384 (Figure 3b, S4b), and Cl occupying the conserved hydrophobic region constituting L446, I/L377 and F472. In contrast, **13** and **14** failed to dock into the receptor. A possible explanation for this result is that the hydrophobic area as seen in docked **15**/**16** clashes with the polar –NH_2 group in **13**/**14**. Apart from the total score, SYBYL Surflex-Dock also provides a crash score (degree of inappropriate penetration by the ligand into the protein and of interpenetration between ligand atoms or self-clash that are separated by rotatable bonds). A crash score close to 0 is favorable, while negative numbers indicate penetration. These scores can be highly useful to have deeper understanding of favorable or failed docking outcomes. For both **13** and **14**, the crash value was ≤ –4.0, which suggests that the ligand atoms clashed with the residues in the ATP domain (Table S2).

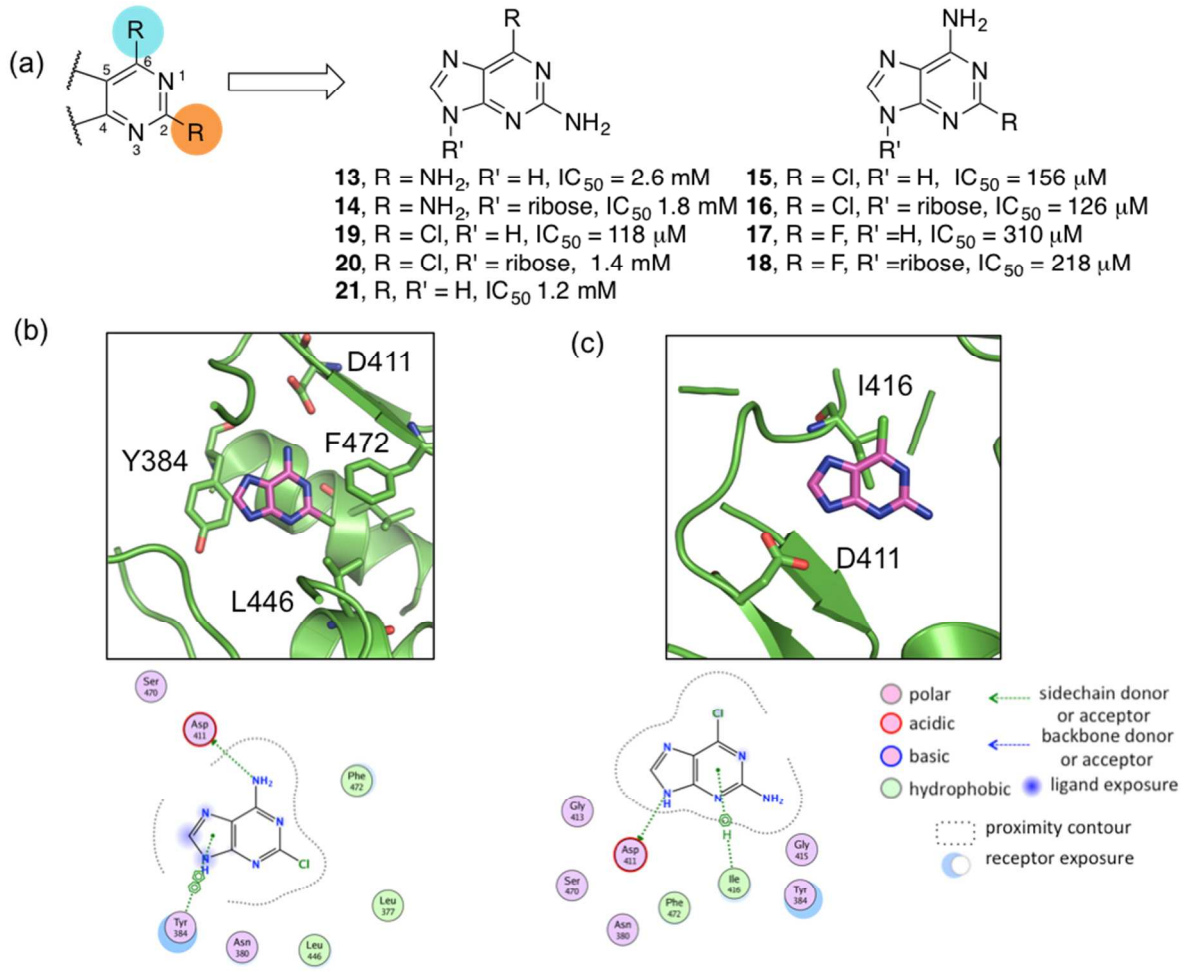

Figure 3. a) HK853 inhibitory activity of adenine compounds with pyrimidine ring modifications. Docking of compounds **15** (b) and **19** (c). The top images show the docking pose of the compound in the receptor cavity. For clarity, only the cavity (green ribbons), and not the full protein, is shown, including important residues (sticks) for ligand-protein binding. The ligands are shown as sticks with C = magenta, N = blue, Cl = green. These images were produced with PyMOL after docking was performed in SYBYL Surflex-Dock. The lower ligand–protein interactions were generated with MOE program. Legend of the possible ligand interactions generated by MOE.

Next, we sought to investigate if swapping the 2-C-Cl and 6-C-NH_2 groups would have

effects on inhibitor activity. The purine, 2-amino,6-chloropurine (**19** IC_{50} 118 μM) has better affinity than adenine (**5**), and is slightly more potent than the 2-Cl analog **15** (Figure 3a, Table 1). Compound **19** was then docked using the same protocol (Figure 3c). Interestingly, a binding pose more similar to that of leads **1** or **3** where 9-NH- makes polar contacts with D411 was observed, even in the presence of a free primary amine at 2-C-NH_2. If this interaction is present, then the riboside, 2-amino,6-chloropurine ribose (**20**) should show no activity, which is what is observed in our biochemical assay (IC_{50} 1.4 mM) and docking experiments (ligand failed to dock; Figure 3). This result reinforce that the crucial H-bonding interaction to the Asp in HKs is through the 9-NH and not through 2-C-NH_2, unless the ribose causes unfavorable interactions. A similar low affinity was seen with 2-aminopurine (**21**), which is not substituted at 6-C and has a 2-C-NH_2, thereby indicating that this amine is incapable of binding to D411. Finally, if the inhibitor binds through the 9-NH, other binding events to the conserved G415 and N380 as seen with ADP, can occur through the nearby N atoms (like 3-N or 7-N). We estimate that these additional contacts make the flipped pose of inhibitors **1**, **3** or **19** highly favorable and possibly in **2**/**4**. In summary, these studies indicate that a chloro substituent on the adenine greatly enhances its activity, and is preferred on both the 2-C and 6-C positions, although the binding poses are different for the resulting inhibitors.

Since the lead compounds (**1**, **2**, **3**, **4**) and the superior inhibitor **19** had 6-C functionalization, we next explored this position on the ring. Examination of the 15 additional adenine-like hits for the HTS indicated that large, hydrophobic groups at C-6 often result in protein aggregation at low concentrations (~100 μM; compounds referred to as non-leads, **NL**-; representative examples in Figure 4a, all in Figure S7). Thus, we pursued variants that are similar in size to lead **4** such as the bioisosteric analog **22** (Figure 4a, Table 1). Bioisosteres or structural

motifs that are similar in shape and function have proven to enhance potency and/or pharmacological properties.[38] Gratifyingly, we observed that placement of an aniline group on 6-C, 6-anilinopurine (**22**) had superior potency (IC_{50} 7.3 μM) compared to **3** and **9** by nearly 20- and 60-fold, respectively. This increase can be attributed to the electron delocalizing effect resulting in H-bond and/or enhanced hydrophobic interactions with the aniline group. To determine if the analog binds to D411 through 9-NH like **3**, we synthesized the riboside, 6-anilinopurine ribose (**23**). This analog failed to inhibit the HK, confirming our hypothesis that when the 6-N position is functionalized with an alkyl group, the binding pose preferred by the adenine base is likely one where it donates a H-bond to the Asp through 9-NH. Upon docking **22**, a similar observation was made with 9-NH–D411 and an additional arene-H interaction was seen with conserved V431 in the ATP lid (Figure 4b, Table 1). Importantly, this compound does not aggregate HK853 even at ≥1.25 mM (See aggregation analysis section in SI).

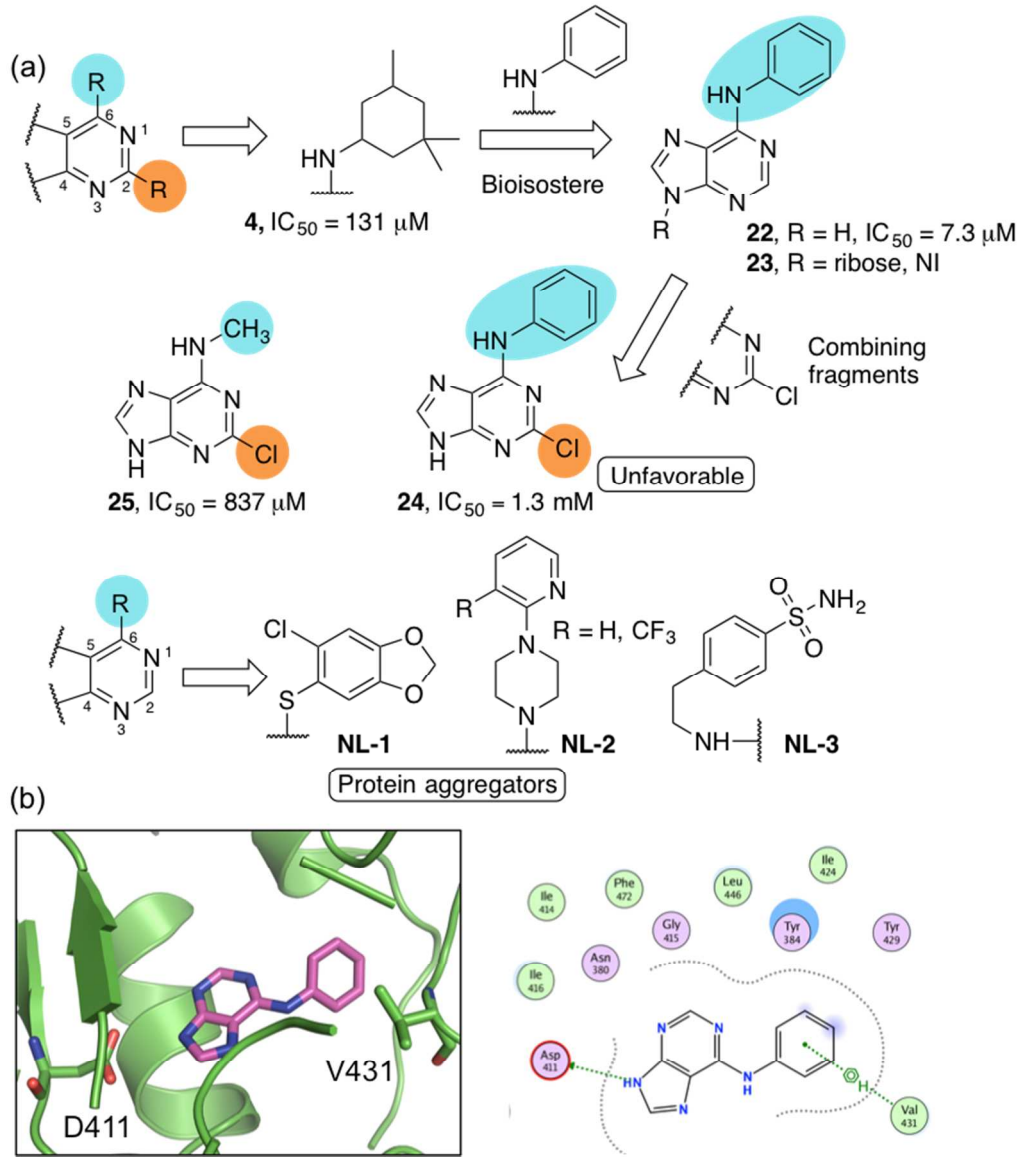

Figure 4. a) HK853 inhibitory activity of adenine-like compounds with pyrimidine ring modifications. b) Docking pose of compound **22**. The left image shows the docking pose of the compound in the receptor cavity. For clarity purposes, only the receptor cavity (green ribbons) and not the full protein, along with the important residues (sticks) participating in the ligand-protein binding, are shown. The ligands are shown as sticks with C = magenta, N = blue. The right image was produced with PyMOL after docking was performed in SYBYL Surflex-Dock. The images are ligand-protein interactions were generated with MOE program. Legend of the

possible ligand interactions generated by MOE.

At this stage, placement of an anilino group at 6-C and chloro at 2-C resulted in superior activities for adenine inhibitors. However, these compounds employed opposite docking poses to interact with D411 indicating that the combination of these two features may yield a poor binder. We synthesized 2-chloro,6-anilinopurine (**24**) by an electrophilic substitution on 1, 2-dichloropurine with aniline and as predicted, found it to be far less potent (IC_{50} 1.3 mM) than **22** or **15** (Figure 4a, Table 1). Even addition of a small group, such as methyl, at 6-C-NH in combination with the 2-Cl yielded an inferior inhibitor, 2-chloro,6-*N*-methyladenine (**25**; IC_{50} 837 μM) in comparison to **15** or **9**. Consistent with these data, when ligand **24** was docked into HK853, it attained a unique binding pose in which the 9-NH weakly interacts with Y429 and contacts with D411 are no longer observed (Figure S4c). During the preparation of **24**, we obtained the di-substituted adenine derivative (**S1**) as a by-product. We tested the potency of this compound (Table S1) and found it to exhibit much worse inhibition than **24** (IC50 7 mM), suggesting that the additional bulky group at the 2-C position is highly unfavorable.

Evaluation of Imidazole Substitutions

After exploring the pyrimidine ring of the adenine core, we next focused on the pyrrole ring system. The 7-N of the pyrrole ring of ADP is predicted to form a water-mediated H-bond to conserved N380 and we postulated that this residue is vital for nucleotide-binding as it likely also interacts with ribose, the phosphates and Mg^{2+} (Figure 1b). Mutation of the analogous amino acid, N347D, in EnvZ (*E. coli*) by Tanaka and coworkers demonstrated that substituting this important residue causes complete loss of ATP binding and autophosphorylation activity.[39] We do not observe these interactions in our docking studies as they were performed following the removal of water molecules from the active site. Nevertheless, residues N380 and G415 are often

situated in close proximity to the docked poses of our leads (within 3-7Å). To further assess the importance of 7-N to productive binding, we examined analog 7-*N*-methyladenine (**26**), in which the nitrogen has been methylated (Figure 5a, Table 1). As expected, **26** failed to show any activity indicating that the free 7-N is vital. We also noted that the 2-*N,N*-dimethyl amino version (Figure S8) was a non-hit (**NH**) in our HTS pilot screen. When the methyl group is instead positioned on 9-N, the resulting compound 9-*N*-methyladenine (**27**) is more potent than unmodified base **9** and possibly interacts with the active site in a similar orientation. These data suggest that the combination of *N*-methylation and a chloro group at C-2 (e.g., **15**) may yield a more active molecule. As expected, methylation at 7-N resulted in an inactive compound (2-chloro,7-*N*-methyladenine, **28**). Instead, when 9-N was methylated to provide 2-chloro,9-*N*-methyladenine (**29**), we found it to be superior to both **15** and **27** (IC_{50} 95 μM; Figure 5a, Table 1). This observation confirms that in addition to H-bonding interactions with D411, molecule binding is dependent upon interactions with residues such as N380 and G415.

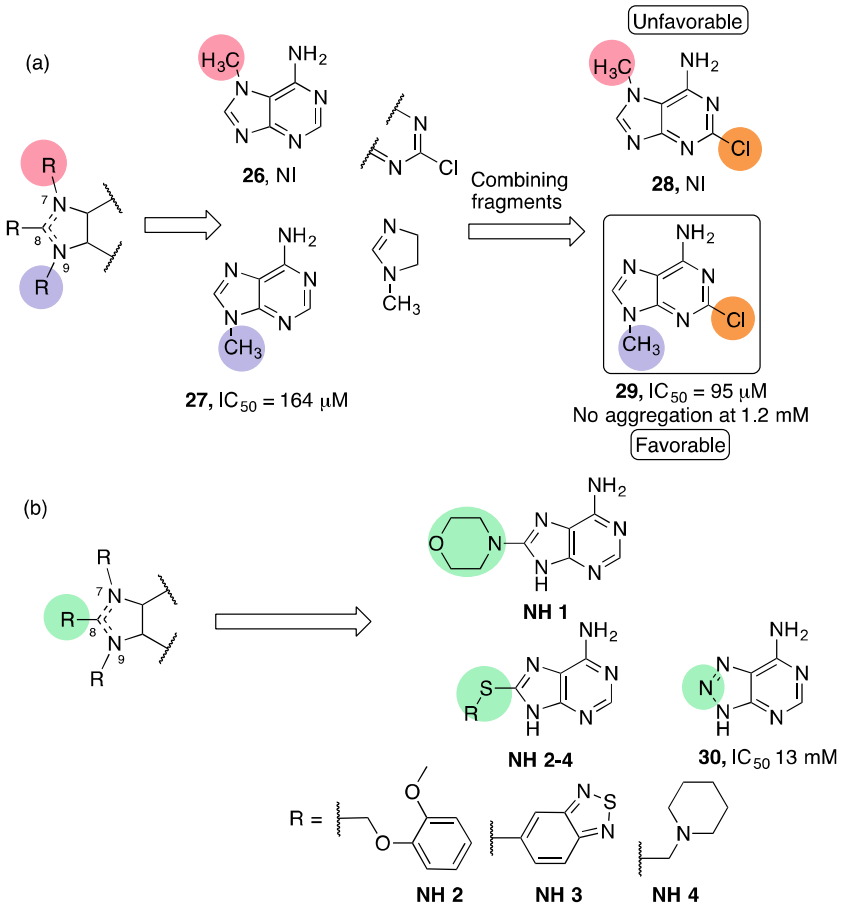

Figure 5. (a) Adenine inhibitors with functionalization at 7-N, 9-N and 2-C positions and their activity for HK853 inhibition. (b) Adenine inhibitors with functionalization at 8-C positions and their activity for HK853 inhibition.

Inhibitor Selectivity Assessment

Inhibitor selectivity is an essential feature of lead compounds, thus, we sought to examine the ability of adenine-based compounds to interact with two important classes of ATP-binding mammalian proteins, HSPs and EKs. EKs or mammalian (Ser/Thr, Tyr) kinases share common features within their catalytic site including several β-sheets that together form a conserved N-lobe, while α-helices constitute the conserved C-lobe and in between these lobes, there is "hinge" region where ATP binds (Figure S9a).[40, 41] These active site features are quite distinct from the

Bergerat fold that is present in HKs. Further exploring one of EK-adenine inhibitor crystal structures (PDB:4XX9, Figure S9b,c)[42] and comparing that to ADP–bound HK structures reveal many differences, providing prospects for the design of selective inhibitors.

Notably, several clinically-utilized drugs that target the EKs are adenine-based and provided the ideal platform to determine if EK inhibitors also interact with the HKs (Figure 6a).[41] These compounds all contain an NH or NH_2 at the 6-C position and most display substituents on the 7, 8, 9-positions of the pyrrole-type ring. The co-crystal structure of B43 (similar to Ibrutinib) with Bruton's tyrosine kinase (BTK) shows H-bonds between the 6-NH and 1-N on the 4-amino pyrrolopyrimidine ring to backbone residues, Glu475 and Met477 (PDB:3GEN, Figure S10b),[43] whereas Idelalisib interacts with phosphoinositide 3-kinase delta (PI3Kδ) by forming an H-bond between V828 and N-3 of the pyrimidine ring (PDB: 4XE0, Figure S10a).[44] Although these structures do not depict a generalized picture of how these two kinase drugs might interact with other EKs, the distinct differences in the inhibitor interactions compared to that of HKs can be observed. Nevertheless, we purchased Idelalisib and Ibrutinib and tested their activity for HK853 inhibition. Both of them failed to show any inhibition even at 1.25 mM, providing evidence that selective inhibition can be attained (HK853 inhibition section in SI). We utilized the structures of these adenine-like kinase drugs to yield a picture of their commonalities as shown in Figure 6a. The pink circle highlights the free amine, the yellow circles show the N-atoms within the scaffold required for protein interactions and the blue arrows indicate the positions on the ring that display substituents. Given the distinct fold that EKs use to bind ATP and the inability of these EK inhibitors to affect the HKs, the likelihood that selectivity for the latter is achievable is high.

We next focused on the GHKL family, specifically HSPs. In the past decade, HSP90

chaperone proteins have become of paramount interest in the field of cancer drug discovery.[45] As HSPs are prime drug targets in humans, attaining selectivity against this class of proteins is of great importance. HSPs and HKs share the Bergerat fold as their adenine-nucleotide-binding pocket indicating that inhibitors of one enzyme type could bind the other favorably (Figure S11). Moreover, within the GHKL family, HKs are structurally closest to HSPs due to their similarities in the flexible ATP-lid. These features prompted us to investigate co-crystal structures of HSP90 to gather information about their ligand-receptor binding. Not surprisingly, many HSP90 inhibitors are derived from a purine-scaffold and several co-crystal structures are available (Figure 6b).[45] Chiosis and coworkers have performed pioneering work in the development of potent adenine-based HSP90 inhibitors and one is in clinical trials as an antitumor agent (Figure 6b, **PU-H71**).[46] Pharmaceutical companies, such as Vernalis, have conducted fragment screens and discovered purine-based hits that are similar to some of our analogs (Figure 6b, **VF**-series). For example, **VF1** is similar to **27** and compound **VF3** displays a 6-C-NH feature as seen in **3** and **29**.[45] Inspection of purine inhibitor-HSP90 co-crystal structures highlights several key interactions, including: 1) H-bond of 9-NH to D93, 2) water-mediated H-bonds with conserved G97 and N51 by the 3-N and 7-N on adenine ring (Figure 7c). These interactions directly correlate with those predicted by our docking and SAR studies with the HKs. In addition, the flipped binding pose that we predicted for analogs **1** and **3** was observed with HSP90 bound to **VF2-3**, where 9-NH interacts with the conserved aspartate (Figure S12). As described in this report,[45] this binding mode enables Gly:Asp:Asn coupling with the 7-N:9-N:3-N triad as seen with the related adenine sites, 1-N:6-C-NH_2:7-N (Both triads are shown in Figure S13 with postulated interactions). The strong similarities between our models of adenine inhibitor-HK binding and published HSP90-ligand structures provides additional evidence for the accuracy of

our SAR-docking results.

We conducted a thorough survey of the published purine-based HSP90 inhibitors that have been developed both commercially and academically.[45-47] Curiously, the inhibitors discovered by Abbott and Biogen bound to the catalytic D93 of mammalian HSP90 through the aminopyrimidine moiety, a position equivalent to 2-C of adenine (Figure 6b).[45, 48] Importantly, similar compounds from our library (**13**, **14**, **20**, **21**) showed negligible activity, with the exception of **19**. A key difference between **19** and the HSP90 analogs is that the main H-bond to the conserved Asp is through 9-NH, whereas in the HSP90 inhibitors it is through 2-C-NH_2. We decided to investigate this feature with other nucleobases, as many of them have an amino-pyrimidine group (Figure 6b). Among these, guanine or guanosine both did not inhibit HK853, indicating that in the presence of a 2-C-NH_2, D411 does not bind indiscriminately to any available –NH on the purine ring. Several unnatural bases (hypoxanthine, inosine) also failed to bind, further indicating that HKs are selective to adenine-like nucleobases and that the presence of a 2-C-NH_2 is disfavored. These results were encouraging towards our effort to identify HK-selective leads.

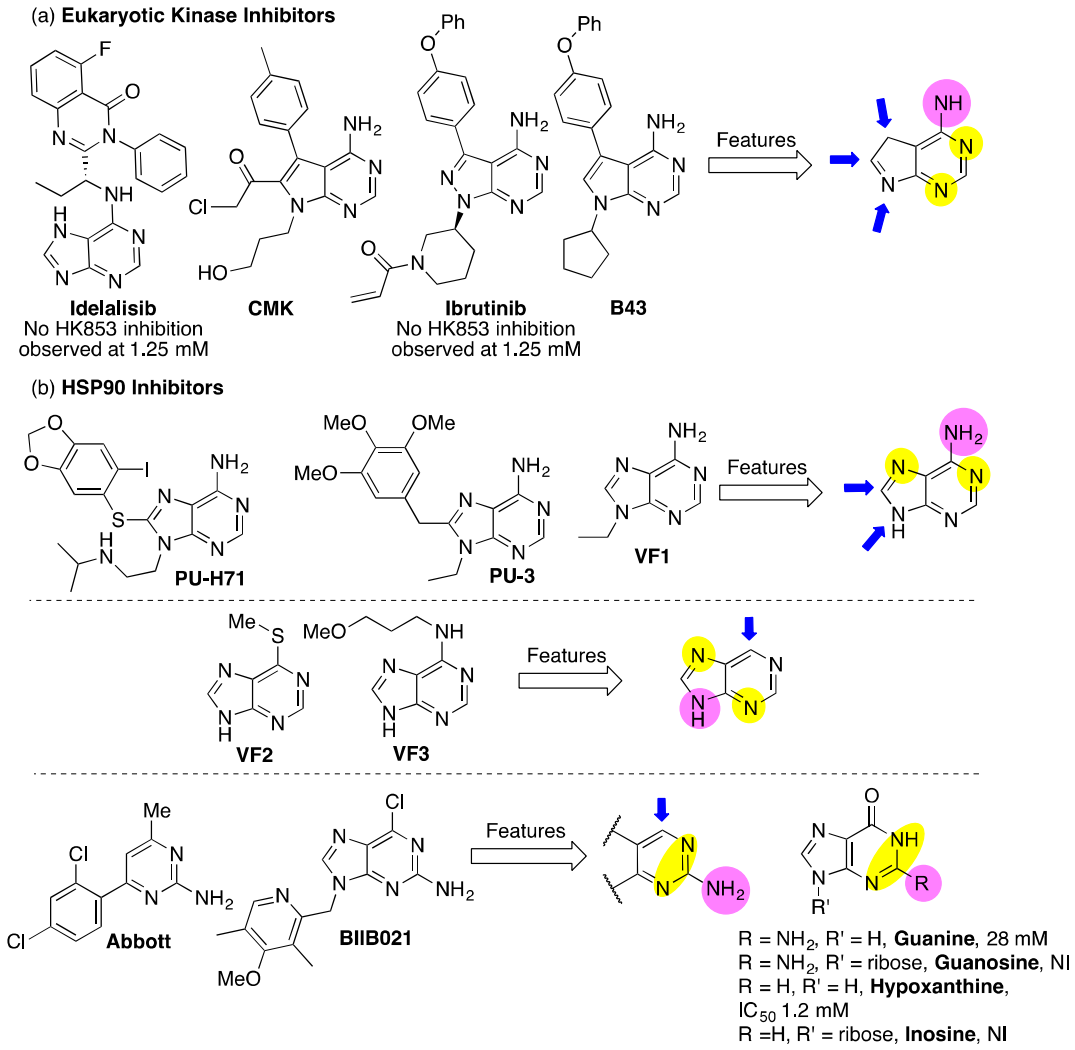

Figure 6. (a) FDA approved EK inhibitors and their HK853 inhibition. (b) Published HSP90 inhibitors. Yellow spheres indicate the similar N-scaffold, pink spheres show the conserved -NH, which forms an H-bond to an Asp residue and the blue arrows indicate substitutions on the ring commonly found in these inhibitors.

We noted several common features in HSP90 adenine inhibitors including a highly functionalized phenyl ring attached at 8-C position (Figure 6b). Since the 8-C on the imidazole core is crucial for HSP90 activity, we sought to determine if such compounds inhibit the HKs. A number of adenine analogs that are functionalized on 8-C were included in our initial HTS and

were all found to be inactive (n=1; representative examples in Figure 5b, all in Figure S8). We also examined the bioisostere, 8-azadenine (**30**), to determine if replacement of the carbon with nitrogen is beneficial and found minimal activity, suggesting that any substitution on the 8-C position yields unfavorable HK interactions. We anticipate that this feature is likely to aid in the design of selective inhibitors for HKs, as most mammalian kinase and HSP90 drugs have 8-C modifications.

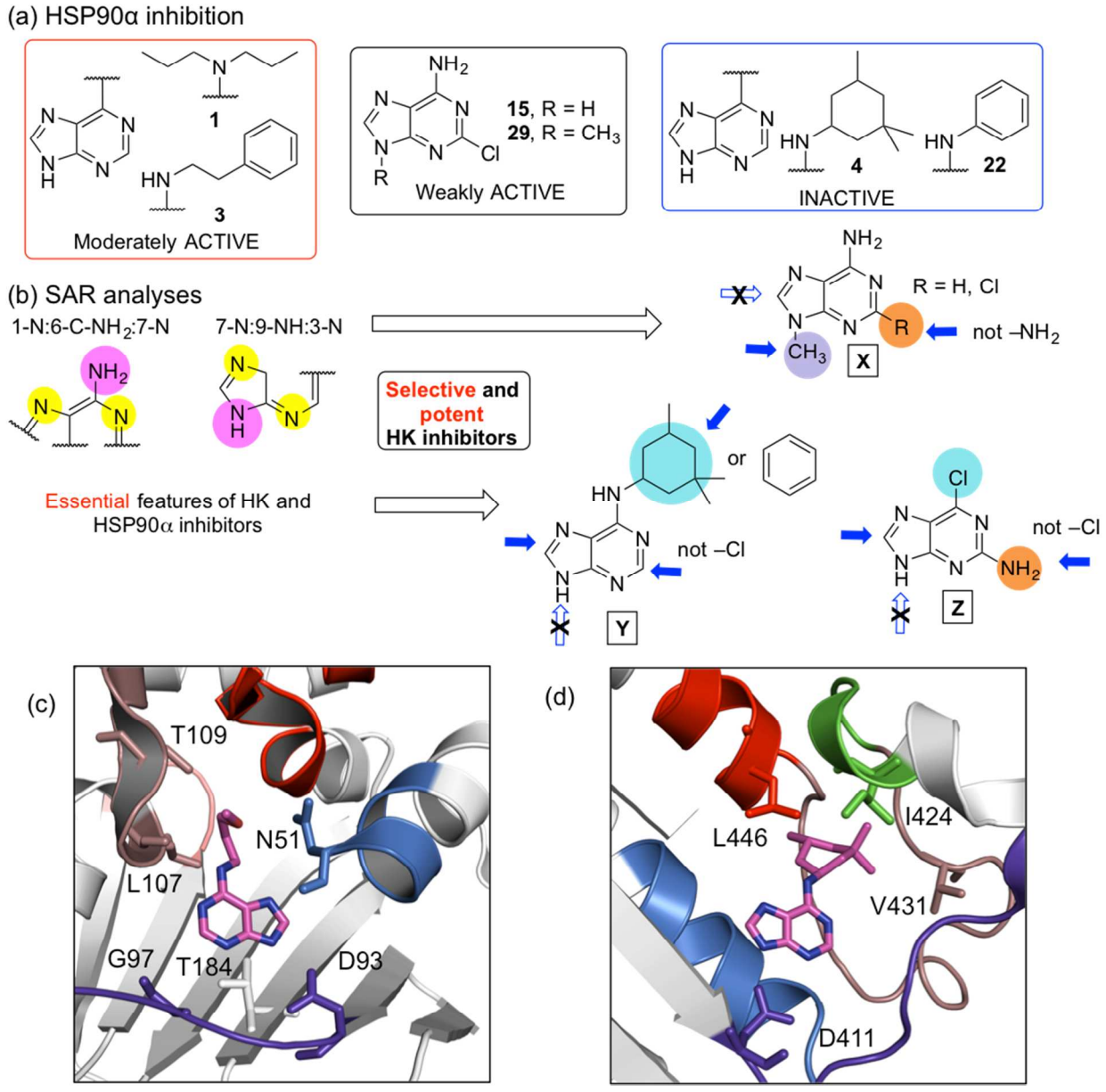

Figure 7. (a) Representative examples of compounds tested for HSP90α inhibition. (b) Combined SAR analyses of all inhibition studies on HKs, EKs, HSP90s yielding selective HK inhibitors. Yellow spheres indicate the similar N-scaffold, pink spheres indicate key NH for Asp interaction, blue arrows indicate the substitutions on the ring to achieve selective HK inhibitors and blue arrows with black crosses indicate substitutions that result in poor inhibition for HKs. (c) Co-crystal structure of HSP90 with compound **VF3** (PDB:2YEH), showing the active site residues interacting with the ligand. The residues belonging to different parts of the Bergerat fold are color-coded, Blue = N-box, Purple = G-1 box, Red = G-2 box, Brown = short α-helix. The red and brown regions constitute the ATP lid domain in HSP90s. (d) Docked pose of compound **4** in HK853 showing key conserved residues that interact with the ligand. The residues belonging to different parts of the Bergerat fold are color-coded, Blue = N-box, Purple = G-1 box, Red = G-2 box, Green = F-box, Brown = flexible loop. The red, green and brown regions constitute the ATP lid domain in HKs.

Although it is important to test HSP90 inhibitors for HK inhibition, it is critical to test the adenine-based HK inhibitors for HSP90 inhibitory activity. To this end, a commercially available FP-based binding assay to assess HSP90α inhibition was utilized to test the efficacy of several of our adenine inhibitors. As outlined in Figure 7a, out of the 13 compounds that were tested, 5 analogs showed inhibition of HSP90 (full compound list in Figure S13; selectivity ratios in Table S6). Compounds **3**, **4** that display long 6-C alkyl or alkyl-phenyl amines and 2-Cl adenosine (**16**) were moderately active (IC_{50} ≤1.25 mM). Whereas, with a $–CH_3$ at the 9-NH position in **29**, this inhibition is reduced (IC_{50} >>1.25 mM), suggesting that this scaffold might be a starting point for generating selectivity. We compared the inhibition activity of **1**, **4**, **16**, **29** for HKs against HSP90 and found that selectivity for the former is high (10-2000 fold; Table S6). Some of the

compounds (**25**, **26**) that were ineffective HK inhibitors were also found to be inactive for HSP90, supporting the similarities in the ligand-binding of these two proteins.

Overall, our studies indicate that one of two adenine N-NH-N fragments is essential for binding to HSP90 and HKs and enabled us to generate three purine-based scaffolds that are potent, as well as selective for bacterial HKs (Figure 7b). The first scaffold (**X**) has the 1-N:6-C-NH_2:7-N design, a $–CH_3$ substituent at 9-N and a 2-Cl group. This core structure can be further modified at the 9-N and 2-C positions to improve potency but not at the C-8 position. The more potent scaffold (**Y**) displays the 7-N:9-NH:3-N triad that has a 6-membered cyclic group at 6-C-NH. This scaffold can be modified at various positions including bioisosteres at the 6-C-NH position and we decided to investigate it further. First, to rationalize the observed selectivity, we examined the co-crystallized structure of **VF3** with HSP90 as it has a 6-C modification like compounds **4** and **22** (Figure 7c, S12c). We compared it to the docked pose of **4** in HK853 (Figure 7d), which was found to be inactive for HSP90. As shown in Figure 7cd, the 9-NH in both compounds forms an H-bond with the conserved Asp (D93, D411) and the exocyclic 6-NH substituents position themselves near the ATP-lid region. It should be noted that although HSPs and HKs share the Bergerat fold, their ATP lid domains are quite distinct. Specifically, the ATP lid in HSP90 is long and comprised of short α-helices, G-2/3 boxes. Whereas in HKs, the ATP lid is much more flexible and has a conserved hydrophobic F-box along with G-2/3 boxes. Our modeling suggests that the cyclohexylamine in **4** (or the Ph ring in **22**) likely accesses the conserved hydrophobic residues (e.g., V431, I424 and L446) on the lid of HK853, which are not found in HSP90. Unlike **4**, the alkyl ether in **VF3** interacts with T109 and L107 from the ATP lid in HSP90. In HKs, this region is more hydrophobic and appears to prefer 6-membered cyclic lipophilic groups. All of these interactions can possibly aid in the selectivity of compounds **4** and

22 for the HKs. Moreover, the size of such a cyclic group likely mimics the ribose in the ADP-pocket, which perhaps allows the optimum positioning of the 6-membered ring in these molecules. Finally, although the simple purine scaffold (**Z**) has some similarities to the aminopyrimidine HSP90 inhibitors reported by Biogen and Abbott, our data indicate that selective HK inhibitors could be obtained with careful design.

Conclusion:

The World Health Organization (WHO) recently published a report on the world's 12 most dangerous superbugs that need immediate attention as treatment options are running out. Most of these antibiotic-resistant strains like MDR *M. tuberculosis* or methicillin-resistant *S. aureus* have TCSs or bacterial kinases that control critical signaling pathways and aid in pathogenicity. We have previously generated diverse leads that can inactivate multiple histidine kinases making them potential antibacterial candidates. In this work, we report a detailed investigation on the SAR studies of one class of these molecules; the adenine-based leads. By doing structure-based design and exploration of substituents on various positions about the adenine ring, we discovered more potent inhibitors. Some key residues such as D411, N380, G415 in HK853 and their interactions with the inhibitors were found to be essential for activity and must be considered in the design of ATP-competitive compounds. Since bacterial kinases are functionally similar to mammalian kinases and structurally related to chaperone heat-shock proteins, the selectivity of the HK inhibitors was also tested. Conducting various inhibition assays and correlating the function of the tested molecules, we constructed three purine-based scaffolds that are not only effective but are also selective for HKs. Efforts are ongoing to study the effects of these inhibitors in both Gram-positive and Gram-negative bacteria.

Experimental Section:

Adenine inhibitor library

All molecules were >95% purity as judged by HPLC analysis (Instrument: Agilent HPLC 1200 series, column: Agilent Eclipse XDB-C18, 5 μm, 9.4x250 mm, gradient run of 20 min with 95% water to 100% acetonitrile, modifier: 0.1% Formic acid)

Compound Synthesis

The *N*-6 substituted purines were synthesized following previous protocols.[49] In brief, to chloropurine or chloropurine riboside was added the amine (3 equiv., 3-5 mmol) and ethanol. This mixture was refluxed overnight (>16 h). After completion of reaction was confirmed by TLC, the solvent was evaporated *in vacuo* and the residue purified by column chromatography with EtOAc:MeOH (gradient solvent from 12:1 to 9:1) as solvent system. For characterization, NMRs were taken on 500 MHz Bruker instrument equipped with a cryoprobe. ESI-MS was performed on an Agilent UPLC-QTOF instrument in positive ionization mode.

6-N,N dipropylaminopurine riboside **12** (white crystalline solid, MP = 136-138°C, 72% yield). HNMR (CD_3CN) ^{1}H NMR (500 MHz, CD_3CN) δ 8.14, 7.92 (2s, 2H, adenine ring Hs), 5.96 – 5.83 (m, 1H, H-1 of ribose), [5.78 (d, J = 7.1 Hz, 1H), 4.82 (td, J = 6.8, 5.0 Hz, 1H), 4.29 (td, J = 3.1, 1.5 Hz, 1H), 4.14 (d, J = 1.6 Hz, 1H), 3.72 – 3.62 (m, 4H), 3.52 (d, J = 3.15 Hz, 1H) ribose ring Hs, 2x -N-C**H$_2$**CH_2CH_3], 1.70 (h, J = 7.4 Hz, 4H, 2x -N-CH_2C**H$_2$**CH_3), 0.93 (t, J = 7.4 Hz, 6H, 2x -N-CH_2CH_2C**H$_3$**).^{13}C NMR (126 MHz, CD_3CN) δ 155.35, 152.35, 150.25, 139.93, 121.68 (5C, adenine ring Cs), 91.43, 88.41, 74.21, 72.89 (5C, ribose ring Cs), 63.61, 11.36 (2C, -N-CH_2**C**H_2**C**H_3). Due to the fast tumbling of tertiary amines -N-**C**H_2 was not observed in the C-NMR. ESI-MS: expected (M+H) = 351.1907, found = 351.1898.

2-Chloro, 6-N anilinopurine riboside **23** (white amorphous solid, 85% yield). HNMR (CD_3CN):

^{1}H NMR CD_3CN) δ 8.38, 8.11 (2s, 2H, adenine ring Hs), 8.26 (s, 1H, -N**H**-Ph), [7.91 – 7.80 (d, *J* = 7.9 Hz 2H), 7.39 (t, *J* = 7.4 Hz, 2H), 7.17 – 7.10 (t, *J* = 7.4 Hz, 1H) Ph ring Hs] , 5.87 (d, *J* = 6.8 Hz, 1H, anomeric H-1 of ribose), [4.80 (t, *J* = 6.0 Hz, 1H), 4.33 (s, 1H), 4.16 (s, 1H), 3.87 – 3.63 (m, 1H), 3.56 (s, 1H), ribose-ring Hs]. ^{13}C NMR (126 MHz, CD_3CN) δ 153.79, 152.72, 149.62, 142.26 (5C, adenine ring Cs), 139.82, 129.64, 124.60, 122.17, 119.45 (4C, Ph-ring Cs), 91.40 (1C, C-1 of ribose), 88.32, 74.75, 72.71, 63.46 (4C, ribose ring Cs). ESI-MS: expected (M+H) = 343.1281, found = 343.1289.

Protein Production

***HK853 overexpression and purification*.** Previous methods developed in our lab were followed to produce and purify the protein.[22, 30] Experimental details can be found in the Supporting Information.

PCR site-directed mutagenesis for generation of HK853 D411N construct.[50] The DNA synthesized for wild-type HK853 was used as a template. Sense and antisense primers that originally coded for D411 were altered to asparagine (Supporting Information Table S3). Primers were ordered from New England Biolabs. Two reactions were prepared in PCR tubes: 2.5 ng HK853 wild-type DNA template, 2.5 μL 2.5 mM dNTPs, 2.5 μL 10 X Pfu buffer, 14.65 μL nuclease-free water, and 0.25 μL 100 X Pfu. To one tube, 2.5 μL of 5 μM mutant sense primer (FHJ086) and 2.5 μL of 5 μM outermost wild-type antisense primer were added. To the other, 2.5 μL of 5 μM outermost wild-type sense primer and 2.5 μL of mutant antisense primer (FHJ087) were added. The final reaction volumes were 25 μL. The PCR reaction was 95 °C for 60 s; 30 cycles of 95°C for 30 s, 56 °C for 120 s, and 72 °C for 90 s; and 72 °C for 360 s. To amplify the mutated template, 0.5 μL of product from both the first and second tubes were mixed with 5.0 μL 2.5 mM dNTPs, 5.0 μL of 5 μM outermost sense primer, 5.0 μL of 5 μM outermost

antisense primer, 5.0 μL of 10 X Pfu buffer, 28.5 μL nuclease-free water, and 0.5 μL 100 X Pfu to a total volume of 50 μL. The same PCR method was run. PCR product was purified, digested, and ligated into the p-His-parallel vector as before.[51] The DNA sequence was confirmed as successful through sequencing at the Indiana Molecular Biology Institute. Additionally, transformation of p-His- parallel-HK853 D411A into *E. coli* strain BL21 (DE3)Rosetta, pLysS, and subsequent protein overexpression and purification were performed as described for wild-type HK853.[30]

Inhibition of HK853 Activity

BODIPY-ATPγS competition screening was performed at inhibitor concentrations that did not cause aggregation. Triton X-100 was premixed with reaction buffer to yield 0.1% (v/v) in final 25-μL reactions. In reaction buffer, 1 μM HK853 was preincubated with test compounds (final concentration, 0.01−1250 μM) in 24 μL for 30 min. 1 μL BODIPY-ATPγS was added to bring the final 25-μL reactions to 0.96 μM HK853 and 2 μM BODIPY-ATPγS in the presence of competitors and 5% DMSO. Samples were mixed and incubated in the dark at RT for 1 h before quenching with 8.6 μL 4× SDS-PAGE sample loading buffer and loading 15 μL on a 10% stacking gel. After SDS-PAGE, in-gel fluorescence detection elucidated HK853 activity, and coomassie staining of the gels ensured even protein loading. Integrated density values of the fluorescent gel bands were normalized as "% Activity" with respect to a control that contained no inhibitor. Data were plotted in GraphPad Prism with relation to the log of molar inhibitor to determine IC_{50} values (Equation 1).

Data analysis. Integrated density measurements of in-gel fluorescence and phosphorescence were performed in ImageJ.[52] Data were prepared and analyzed in GraphPad Prism (version 7.0

for Mac, GraphPad Software, San Diego, California USA, www.graphpad.com). For all DRCs (control FP competition and activity assays), data were fit to a four-parameter logistic equation,

$$y = Bottom + \frac{(Top - Bottom)}{1+10^{\left((LogIC_{50} - x) * HillSlope\right)}} \qquad \text{(Equation 1)}$$

where *y* is the response, *Bottom* and *Top* are plateaus in the units of the y-axis, *x* is the log of the molar concentration of inhibitor, *HillSlope* is the slope of the curve, and IC_{50} is the concentration of compound required for 50% inhibition (a response half way between *Bottom* and *Top*). Some compounds exhibited incomplete DRCs because going to higher concentrations would increase the required DMSO or cause protein aggregation. Visually, this meant there was no curve plateau for the "Bottom" value. However, IC_{50} values were desirable for purposes of comparison to other compounds. As a result, IC_{50} values were estimated by constraining the bottom of the curve to "0."

HK853 Aggregation Analysis

To analyze the propensity for compounds to cause aggregation, each was mixed at six concentrations (0−1250 μM) with purified 0.5 μM HK853 in 25 μL of 20 mM HEPES buffer (5% (v/v) DMSO final). After incubating at RT for 30 min, 8.6 μL native-PAGE sample loading buffer was added, and 15 μL was loaded onto a 7.5% polyacrylamide gel. Proteins were resolved by native-PAGE and silver staining. Compound-induced aggregation was detected by the disappearance of the dimeric HK853 band. NH125 (Tocris Bioscience) was used as a positive aggregation control.

Molecular Docking Studies

All molecular modeling operations were performed using SYBYL X Surflex-Dock through the University of Minnesota's Supercomputing Institute. The protein used for docking was HK853 co-crystallized with ADP (PDB:3DGE). The receptor was prepared by removing co-crystallized

ligands and water molecules followed by the addition of hydrogens using the Prepare Protein Structure tool. Atom types were assigned using the AMBER method and a staged-minimization was performed on the hydrogens. The compounds were prepared prior to docking using the "Sanitize" protocol in the Ligand Structure Preparation tool found in SYBYL, which removed all counter ions and energy was minimized. The docking was done with the surflex-dock default values for threshold, bloat, number of poses. Visualization of docked poses was done using PyMOL and interactions of the protein-ligand with CCG MOE software.[29]

Thermal Shift Assays-Differential Scanning Fluorimetry (DSF) Studies

All DSF measurements were done on 96-well PCR plates on a Bio-Rad MyiQ2 instrument using HEX filter for relative fluorescence quantification. The DSF protocol was developed based on published methods.[32] The final volume of each reaction was 25 μL and the reagents were kept on ice. The wild-type HK853 or the mutant HK853 protein solutions were prepared in reaction buffer to attain a final concentration of 2-5 μM in the reaction. Next, the 1000x SYPRO orange dye (Thermo Fisher) was diluted in water and added to the protein to be finally at 5x concentration. From a 25 mM DMSO stock solutions of inhibitors, 1 μL was added to obtain a final concentration of 1 mM (for negative control, 1 μL of DMSO was added). The reagents were pipetted carefully to mix them properly. The well plate was then sealed with optical PCR seals (Bio-Rad) and centrifuged briefly to ensure the reagents are settled at the bottom of the plate and to remove bubbles. The PCR plate was then run on the instrument for the "melt curve" analysis from 20 °C to 95 °C at 1 °C min^{-1}. The curves were processed in the iQ5 software to obtain the melting temperatures and the graphs were plotted using Microsoft Excel.

HSP90 inhibition assays

The HSP90 inhibition assays were performed with a commercially available fluorescence polarization based Hsp90α Assay Kit from BPS Biosciences according to the instructions provided.[53] The measurements were recorded on a Tecan infinite 500 instrument in Greiner 96 Flat Bottom Black Polystyrol plates at excitation between 475-495 nm and emission between 518-538 nm. The adenine compounds as listed in the scheme below were tested at a concentration of 1.25 mM (n = 3) in the assay. The compounds, which showed inhibition higher than 45% were further tested, dose response curves plotted with 8 concentrations (1-1250 μM) and their IC_{50} values were calculated using Equation 1 with GraphPad Prism software. For many compounds, the curves did not reach a plateau (weak inhibitors) and the IC_{50}s could not be accurately calculated. To validate the accuracy of the Hsp90α assay, a positive control compound, Geldanamycin was purchased and its IC_{50} was also calculated and found to be consistent with literature.[53]

Table 1. Compounds tested for HK853 inhibitory activity and their IC_{50} values.

Main scaffold 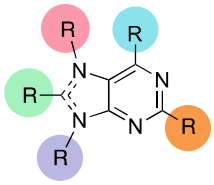	**Previous Leads**[a] 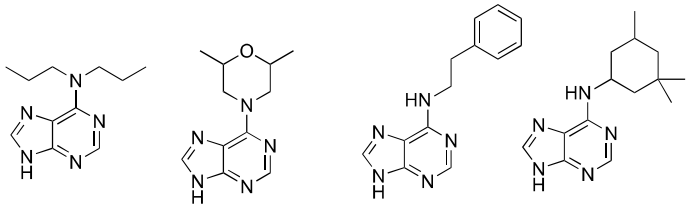 **1,** IC_{50} = 49.6 μM **2,** IC_{50} = 95.3 μM **3,** IC_{50}= 145 μM **4,** IC_{50} = 131 μM	
	This work	
Substructure	*Compound No.*	*IC_{50} values (μM) (95% confidence interval), n = 2*
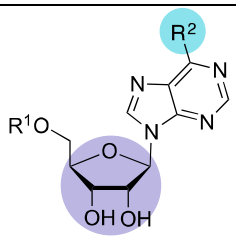	**8,** $R^2 = NH_2$, R^1= H	407 (308-536)
	10, $R^2 = NHCH_2CH_2Ph$, R^1 = H	1790 (1368-2343)
	11, $R^2 = NHCH_2Ph$, $R^1 = 2PO_3^2$	1585 (1217-2065)
	12, $R^2 = NPr_2$, R^1 = H	2683 (991-7257)
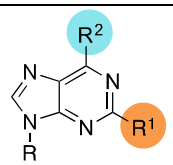	**13**, R^2, $R^1 = NH_2$, R = H	2623 (1671-5487)
	14, R^2, $R^1 = NH_2$, R = ribose	1786 (1244-3256)
	15, $R^2 = NH_2$, R^1 = Cl, R = H	156 (107.4-327.2)
	16, $R^2 = NH_2$, R^1 = Cl, R = ribose	126 (56.0-187.7)
	17, $R^2 = NH_2$, R^1 = F, R = H	310 (110-1897)
	18, $R^2 = NH_2$, R^1 = F, R = ribose	218 (100-3312)
	19, R^2 = Cl, $R^1 = NH_2$, R = H	118 (77-260)
	20, R^2 = Cl, $R^1 = NH_2$, R = ribose	1363 (1117-2128)
	21, R^2 = H, $R^1 = NH_2$, R = H	1207 (917-1950)
	22, R^2 = PhNH, R^1, R = H	7.3 (4.57-104)
	23, R^2 = PhNH, R^1, R = ribose	No Inhibition
	24, R^2 = PhNH, R^1 = Cl, R = H	1283 (835-2566)
	25, $R^2 = CH_3NH$, R^1 = Cl, R = H	837 (700-1004)
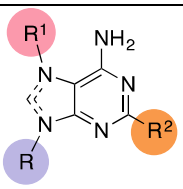	**26,** R^2 = H, $R^1 = CH_3$, R = H	No Inhibition
	27, R^2 = H, R^1 = H, $R = CH_3$	164.2 (116.7-226.5)
	28, R^2 = Cl, $R^1 = CH_3$, R = H	No Inhibition
	29, R^2 = Cl , R^1 = H, $R = CH_3$	95.4 (65.6-190.5)
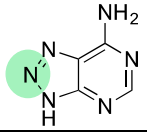	**30**	13660 (2419-18930)
	Guanine	28060 (21710-7.5x10^6)
	Guanosine	No Inhibition
	Hypoxanthine	1199 (944.9-1576)
	Inosine	No Inhibition

ASSOCIATED CONTENT

*Supporting Information

Complete details on methods and results for the following: protein production, compound synthesis and spectra, biochemical assays, docking studies and protein-ligand interactions are provided in the Supporting Information. The molecular formula strings of all the compounds in this work is also available. This material is available free of charge via the Internet at http://pubs.acs.org.

AUTHOR INFORMATION

Corresponding Author

*E-mail: carlsone@umn.edu.

Present Address

Department of Chemistry, University of Minnesota, 207 Pleasant St. SE, Minneapolis, MN 55455, United States.

Notes

The authors declare no competing financial interest.

ACKNOWLEDGMENTS

We thank W. Pomerantz for use of a microplate reader. Indiana University's Physical Biochemistry Instrumentation Facility and the Indiana Molecular Biology Institute provided essential instrumentation. This work was supported by the National Institutes of Health (NIH) DP2OD008592, a Pew Biomedical Scholar Award (E.E.C.), Alfred P. Sloan Fellowship (E.E.C.), an Indiana University Quantitative and Chemical Biology training fellowship (K.E.W.) and the University of Minnesota. We would like to thank University of Minnesota's

Supercomputing Institute for the use of various molecular modeling software.

ABBREVIATIONS USED

Histidine kinases (HKs); catalytic and ATP-binding (CA); Heat Shock Protein 90 (HSP90); two-component systems (TCSs); response regulators (RRs); dimerization and histidine phosphotransfer (DHp); multidrug resistance (MDR); fluorescence polarization (FP); GHKL (Gyrase, Heat shock proteins, histidine Kinase, MutL); eukaryotic kinases (EKs); Molecular Operating Environment (MOE); differential scanning fluorimetry (DSF).

REFERENCES

1. Beceiro, A.; Tomás, M.; Bou, G. Antimicrobial resistance and virulence: A successful or deleterious association in the bacterial world? *Clin. Microbiol. Rev.* **2013,** *26*, 185-230.

2. Clatworthy, A. E.; Pierson, E.; Hung, D. T. Targeting virulence: A new paradigm for antimicrobial therapy. *Nat. Chem. Biol.* **2007,** *3*, 541-548.

3. Heras, B.; Scanlon, M. J.; Martin, J. L. Targeting virulence not viability in the search for future antibacterials. *Br. J. Clin. Pharmacol.* **2015,** *79*, 208-215.

4. Ruer, S.; Pinotsis, N.; Steadman, D.; Waksman, G.; Remaut, H. Virulence-targeted antibacterials: Concept, promise, and susceptibility to resistance mechanisms. *Chem. Biol. Drug Des.* **2015,** *86*, 379-399.

5. Mellbye, B.; Schuster, M. The sociomicrobiology of antivirulence drug resistance: A proof of concept. *mBio* **2011,** *2*, e00131-11.

6. Rasko, D. A.; Sperandio, V. Anti-virulence strategies to combat bacteria-mediated disease. *Nat. Rev. Drug Discovery* **2010,** *9*, 117-128.

7. Stephenson, K.; Hoch, J. A. Virulence- and antibiotic resistance-associated two-component signal transduction systems of Gram-positive pathogenic bacteria as targets for antimicrobial therapy. *Pharmacol. Ther.* **2002,** *93*, 293-305.

8. Beier, D.; Gross, R. Regulation of bacterial virulence by two-component systems. *Curr. Opin. Microbiol.* **2006,** *9*, 143-152.

9. Liu, Q.; Yeo, W. S.; Bae, T. The SaeRS two component system of *Staphylococcus aureus*. *Genes* **2016,** *7*, 81.

10. Gonzalo Asensio, J.; Maia, C.; Ferrer, N. L.; Barilone, N.; Laval, F.; Soto, C. Y.; Winter,

N.; Daffe, M.; Gicquel, B.; Martin, C.; Jackson, M. The virulence-associated two-component PhoP-PhoR system controls the biosynthesis of polyketide-derived lipids in *Mycobacterium tuberculosis*. *J. Biol. Chem.* **2006,** *281*, 1313-1316.

11. Cegelski, L.; Marshall, G. R.; Eldridge, G. R.; Hultgren, S. J. The biology and future prospects of antivirulence therapies. *Nat. Rev. Micro.* **2008,** *6*, 17-27.

12. Dickey, S. W.; Cheung, G. Y. C.; Otto, M. Different drugs for bad bugs: Antivirulence strategies in the age of antibiotic resistance. *Nat. Rev. Drug Discovery* **2017,** *16*, 457-471.

13. Gotoh, Y.; Eguchi, Y.; Watanabe, T.; Okamoto, S.; Doi, A.; Utsumi, R. Two-component signal transduction as potential drug targets in pathogenic bacteria. *Curr. Opin. Microbiol.* **2010,** *13*, 232-239.

14. Johnson, B. K.; Abramovitch, R. B. Small molecules that sabotage bacterial virulence. *Trends Pharmacol. Sci.* **2017,** *38*, 339-362.

15. Rasko, D. A.; Moreira, C. G.; Li, D. R.; Reading, N. C.; Ritchie, J. M.; Waldor, M. K.; Williams, N.; Taussig, R.; Wei, S.; Roth, M.; Hughes, D. T.; Huntley, J. F.; Fina, M. W.; Falck, J. R.; Sperandio, V. Targeting QseC signaling and virulence for antibiotic development. *Science* **2008,** *321*, 1078-1080.

16. Bem, A. E.; Velikova, N.; Pellicer, M. T.; Baarlen, P. v.; Marina, A.; Wells, J. M. Bacterial histidine kinases as novel antibacterial drug targets. *ACS Chem. Bio.* **2015,** *10*, 213-224.

17. Casino, P.; Rubio, V.; Marina, A. Structural insight into partner specificity and phosphoryl transfer in two-component signal transduction. *Cell* **2009,** *139*, 325-36.

18. Galbusera, E.; Renzoni, A.; Andrey, D. O.; Monod, A.; Barras, C.; Tortora, P.; Polissi, A.; Kelley, W. L. Site-specific mutation of *Staphylococcus aureus* VraS reveals a crucial role for

the VraR-VraS sensor in the emergence of glycopeptide resistance. *Antimicrob. Agents Chemother.* **2011,** *55*, 1008-1020.

19. Su, J.; Iehara, M.; Yasukawa, J.; Matsumoto, Y.; Hamamoto, H.; Sekimizu, K. A novel mutation in the *vraS* gene of *Staphylococcus aureus* contributes to reduce susceptibility against daptomycin. *J. Antibiot.* **2015,** *68*, 646-648.

20. Velikova, N.; Fulle, S.; Manso, A. S.; Mechkarska, M.; Finn, P.; Conlon, J. M.; Oggioni, M. R.; Wells, J. M.; Marina, A. Putative histidine kinase inhibitors with antibacterial effect against multi-drug resistant clinical isolates identified by in vitro and in silico screens. *Sci. Rep.* **2016,** *6*, 26085.

21. Boibessot, T.; Zschiedrich, C. P.; Lebeau, A.; Bénimèlis, D.; Dunyach-Rémy, C.; Lavigne, J.-P.; Szurmant, H.; Benfodda, Z.; Meffre, P. The rational design, synthesis, and antimicrobial properties of thiophene derivatives that inhibit bacterial histidine kinases. *J. Med. Chem.* **2016,** *59*, 8830-8847.

22. Wilke, K. E.; Francis, S.; Carlson, E. E. Inactivation of multiple bacterial histidine kinases by targeting the ATP-binding domain. *ACS Chem. Bio.* **2015,** *10*, 328-335.

23. Dutta, R.; Inouye, M. GHKL, an emergent ATPase/kinase superfamily. *Trends Biochem. Sci* **2000,** *25*, 24-28.

24. Welsch, M. E.; Snyder, S. A.; Stockwell, B. R. Privileged scaffolds for library design and drug discovery. *Curr. Opin. Chem. Biol.* **2010,** *14*, 347-361.

25. Francis, S.; Wilke, K. E.; Brown, D. E.; Carlson, E. E. Mechanistic insight into inhibition of two-component system signaling. *Med. Chem. Comm.* **2013,** *4*, 269-277.

26. Celikel, R.; Veldore, V. H.; Mathews, I.; Devine, K. M.; Varughese, K. I. ATP forms a stable complex with the essential histidine kinase WalK (YycG) domain. *Acta Cryst. D* **2012,** *68*,

839-845.

27. Marina, A.; Mott, C.; Auyzenberg, A.; Hendrickson, W. A.; Waldburger, C. D. Structural and mutational analysis of the PhoQ histidine kinase catalytic domain: Insight into the reaction mechanism. *J. Biol. Chem.* **2001,** *276*, 41182-41190.

28. Marina, A.; Waldburger, C. D.; Hendrickson, W. A. Structure of the entire cytoplasmic portion of a sensor histidine-kinase protein. *EMBO J.* **2005,** *24*, 4247-4259.

29. Molecular Operating Environment (MOE), C. C. G. U., 1010 Sherbooke St. West, Suite #910, Montreal, QC, Canada, H3A 2R7, 2017.

30. Wilke, K. E.; Francis, S.; Carlson, E. E. Activity-based probe for histidine kinase signaling. *J. Am. Chem. Soc.* **2012,** *134*, 9150-9153.

31. Chilton, M.; Clennell, B.; Edfeldt, F.; Geschwindner, S. Hot-spotting with thermal scanning: A ligand- and structure-independent assessment of target ligandability. *J. Med. Chem.* **2017,** *60*, 4923-4931.

32. Niesen, F. H.; Berglund, H.; Vedadi, M. The use of differential scanning fluorimetry to detect ligand interactions that promote protein stability. *Nat. Protoc.* **2007,** *2*, 2212-2221.

33. Robinson-Rechavi, M.; Godzik, A. Structural genomics of *Thermotoga maritima* proteins shows that contact order is a major determinant of protein thermostability. *Structure* **2005,** *13*, 857-860.

34. Guarnieri, M. T.; Zhang, L.; Shen, J.; Zhao, R. The HSP90 inhibitor radicicol interacts with the ATP-binding pocket of bacterial sensor kinase PhoQ. *J. Mol. Biol.* **2008,** *379*, 82-93.

35. Ma, S.; Wozniak, D. J.; Ohman, D. E. Identification of the histidine protein kinase KinB in *Pseudomonas aeruginosa* and its phosphorylation of the alginate regulator AlgB. *J. Biol. Chem.* **1997,** *272*, 17952-17960.

36. Reichelová, V.; Albertioni, F.; Liliemark, J. Hydrophobicity parameters of 2-chloro-2′-deoxyadenosine and some related analogues and retention in reversed-phase liquid chromatography. *J. Chromatogr. A* **1994,** *667*, 37-45.

37. Hunter, C. A.; Lawson, K. R.; Perkins, J.; Urch, C. J. Aromatic interactions. *J. Chem. Soc. Perkin Trans. 2* **2001**, 651-669.

38. Patani, G. A.; LaVoie, E. J. Bioisosterism: A rational approach in drug design. *Chem. Rev.* **1996,** *96*, 3147-3176.

39. Tanaka, T.; Saha, S. K.; Tomomori, C.; Ishima, R.; Liu, D.; Tong, K. I.; Park, H.; Dutta, R.; Qin, L.; Swindells, M. B.; Yamazaki, T.; Ono, A. M.; Kainosho, M.; Inouye, M.; Ikura, M. NMR structure of the histidine kinase domain of the e. Coli osmosensor EnvZ. *Nature* **1998,** *396*, 88-92.

40. Kornev, A. P.; Haste, N. M.; Taylor, S. S.; Ten Eyck, L. F. Surface comparison of active and inactive protein kinases identifies a conserved activation mechanism. *Proc. Natl. Acad. Sci. U.S.A.* **2006,** *103*, 17783-17788.

41. Wu, P.; Nielsen, T. E.; Clausen, M. H. FDA-approved small-molecule kinase inhibitors. *Trends Pharmacol. Sci.* **2015,** *36*, 422-439.

42. Rettenmaier, T. J.; Sadowsky, J. D.; Thomsen, N. D.; Chen, S. C.; Doak, A. K.; Arkin, M. R.; Wells, J. A. A small-molecule mimic of a peptide docking motif inhibits the protein kinase PDK1. *Proc. Natl. Acad. Sci. U.S.A.* **2014,** *111*, 18590-18595.

43. Marcotte, D. J.; Liu, Y.-T.; Arduini, R. M.; Hession, C. A.; Miatkowski, K.; Wildes, C. P.; Cullen, P. F.; Hong, V.; Hopkins, B. T.; Mertsching, E.; Jenkins, T. J.; Romanowski, M. J.; Baker, D. P.; Silvian, L. F. Structures of human Bruton's tyrosine kinase in active and inactive conformations suggest a mechanism of activation for TEC family kinases. *Protein Sci.* **2010,** *19*,

429-439.

44. Somoza, J. R.; Koditek, D.; Villaseñor, A. G.; Novikov, N.; Wong, M. H.; Liclican, A.; Xing, W.; Lagpacan, L.; Wang, R.; Schultz, B. E.; Papalia, G. A.; Samuel, D.; Lad, L.; McGrath, M. E. Structural, biochemical, and biophysical characterization of idelalisib binding to phosphoinositide 3-kinase δ. *J. Biol. Chem.* **2015,** *290*, 8439-8446.

45. Roughley, S. D.; Hubbard, R. E. How well can fragments explore accessed chemical space? A case study from heat shock protein 90. *J. Med. Chem.* **2011,** *54*, 3989-4005.

46. Jhaveri, K.; Taldone, T.; Modi, S.; Chiosis, G. Advances in the clinical development of heat shock protein 90 (HSP90) inhibitors in cancers. *Biochim. Biophys. Acta* **2012,** *1823*, 742-755.

47. Verma, S.; Goyal, S.; Jamal, S.; Singh, A.; Grover, A. HSP90: Friends, clients and natural foes. *Biochimie* **2016,** *127*, 227-240.

48. Kasibhatla, S. R.; Hong, K.; Biamonte, M. A.; Busch, D. J.; Karjian, P. L.; Sensintaffar, J. L.; Kamal, A.; Lough, R. E.; Brekken, J.; Lundgren, K.; Grecko, R.; Timony, G. A.; Ran, Y.; Mansfield, R.; Fritz, L. C.; Ulm, E.; Burrows, F. J.; Boehm, M. F. Rationally designed high-affinity 2-amino-6-halopurine heat shock protein 90 inhibitors that exhibit potent antitumor activity. *J. Med. Chem.* **2007,** *50*, 2767-2778.

49. Laufer, S. A.; Domeyer, D. M.; Scior, T. R. F.; Albrecht, W.; Hauser, D. R. J. Synthesis and biological testing of purine derivatives as potential ATP-competitive kinase inhibitors. *J. Med. Chem.* **2005,** *48*, 710-722.

50. Heckman, K. L., Pease, L. R. Gene splicing and mutagenesis by pcr-driven overlap extension. *Nat. Protoc.* **2007,** *2*, 924-932.

51. Sheffield, P., Garrard, S., Derewanda, Z. Overcoming expression and purification

problems of RhoGDI using a family of "parallel" expression vectors. *Protein Expr. Purif.* **1999,** *15* 34-39.

52. Schneider, C. A.; Rasband, W. S.; Eliceiri, K. W. NIH image to imageJ: 25 years of image analysis. *Nat. Methods* **2012,** *9*, 671-675.

53. Joungnam, K.; Sara, F.; Laura, L.; Huazhong, H.; Henri, H.; Neal, R.; Gabriela, C. Development of a fluorescence polarization assay for the molecular chaperone HSP90. *J. Biomol. Screening* **2004,** *9*, 375-38

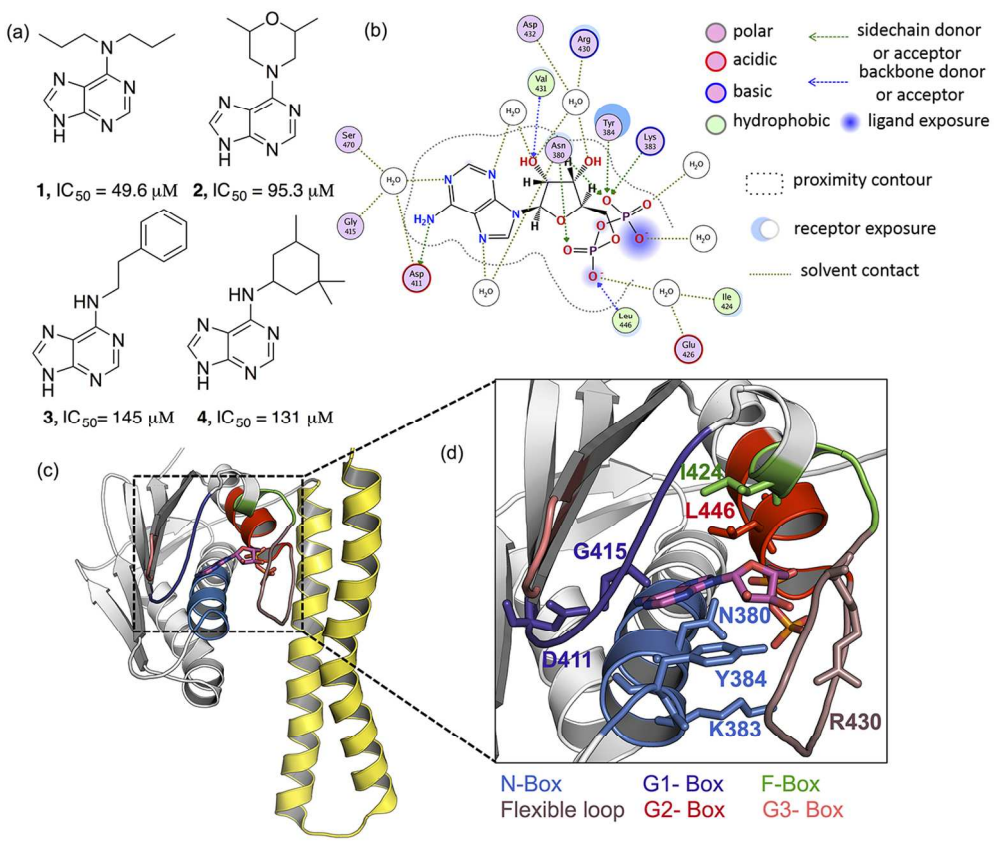

127x106mm (300 x 300 DPI)

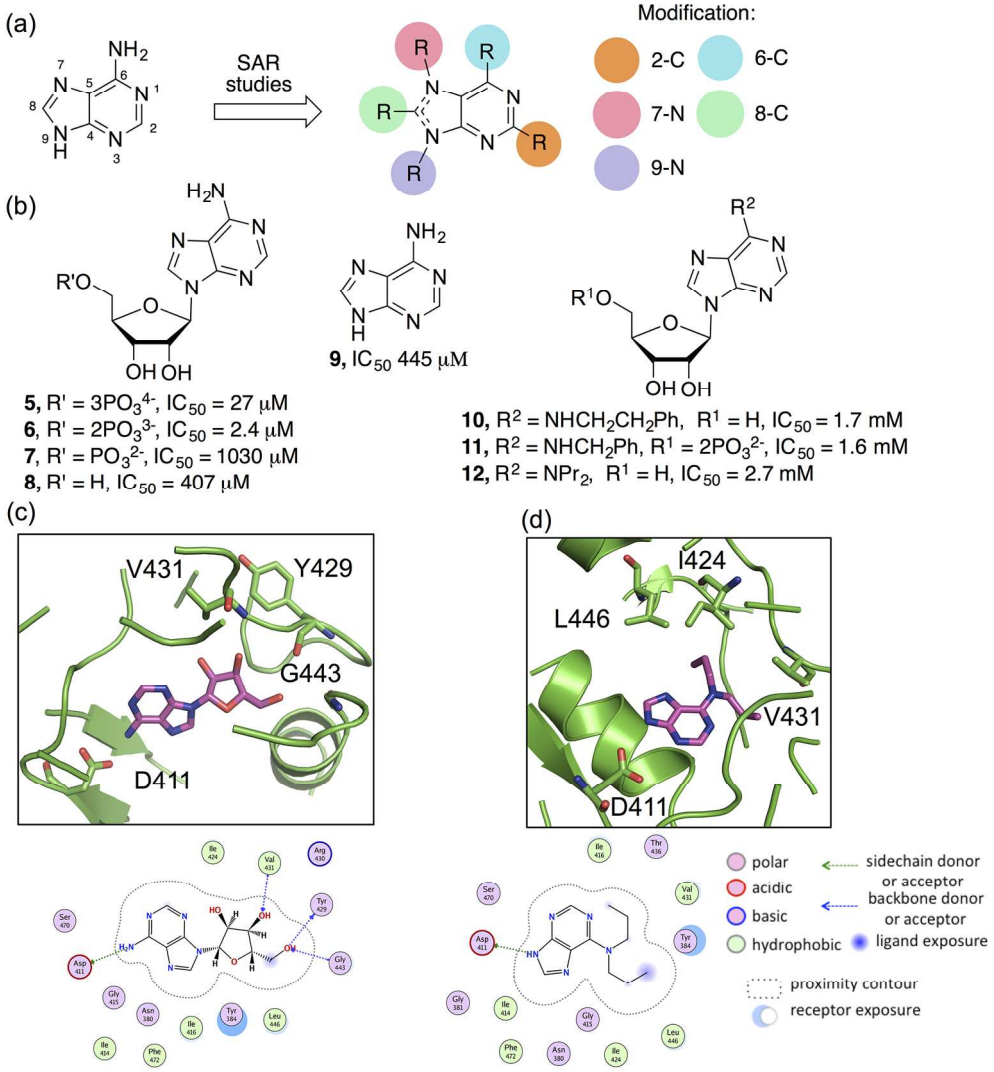

167x181mm (300 x 300 DPI)

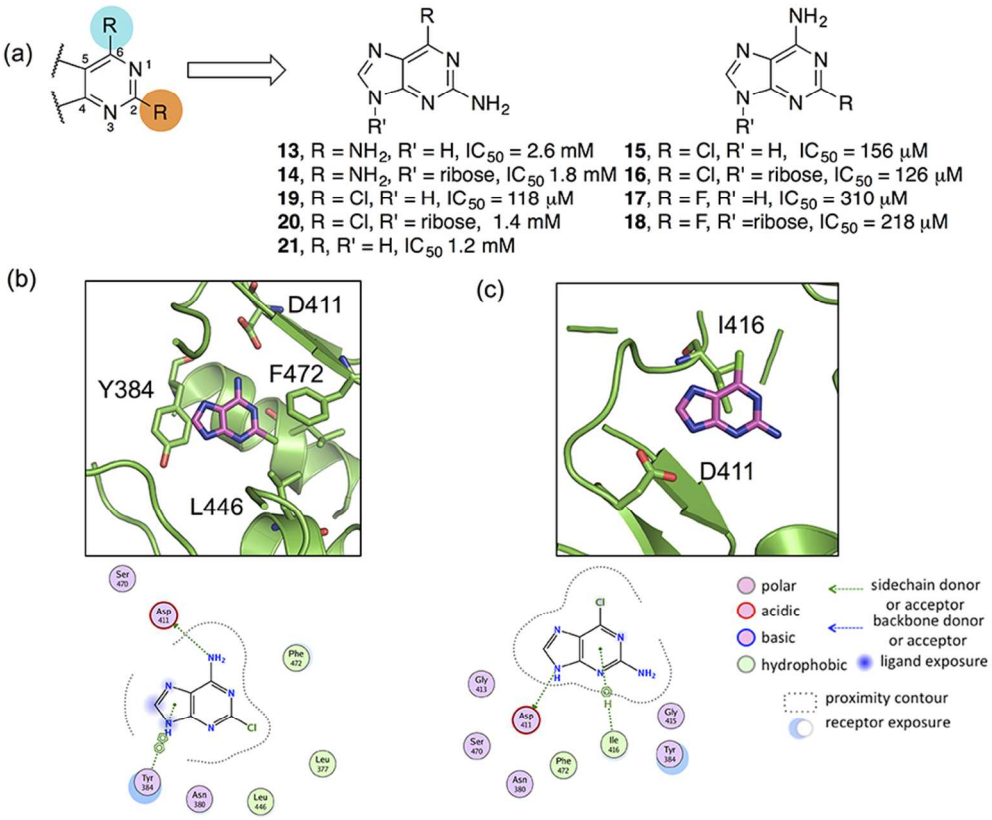

84x70mm (300 x 300 DPI)

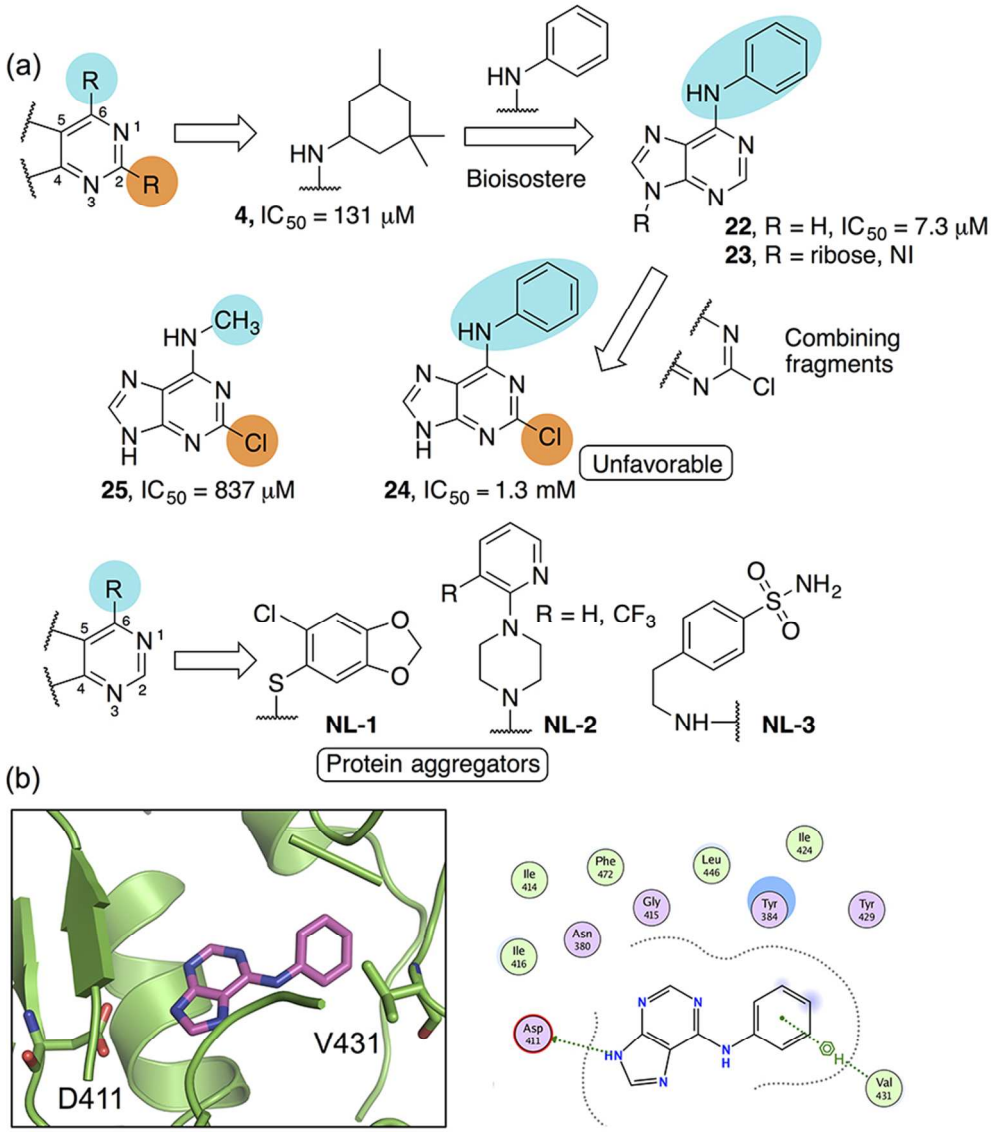

84x97mm (300 x 300 DPI)

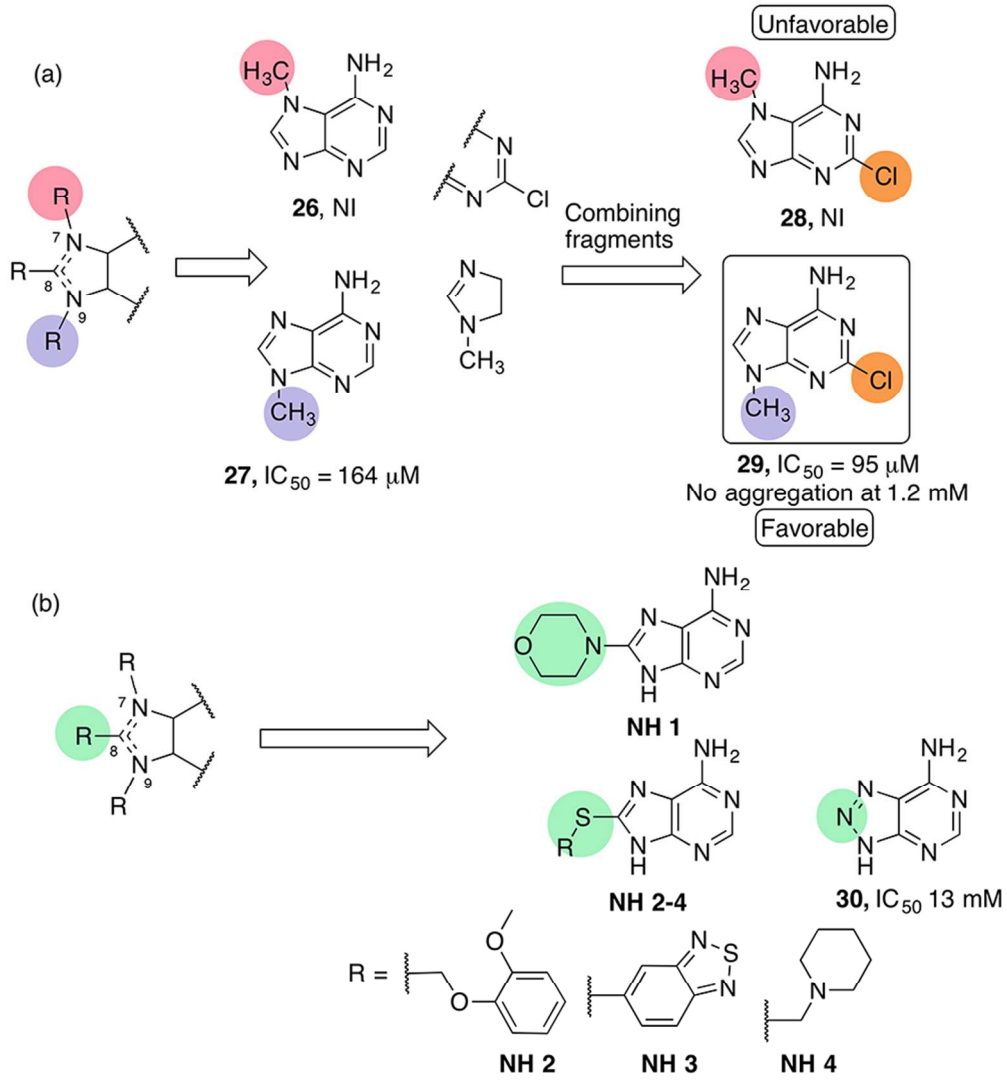

84x91mm (300 x 300 DPI)

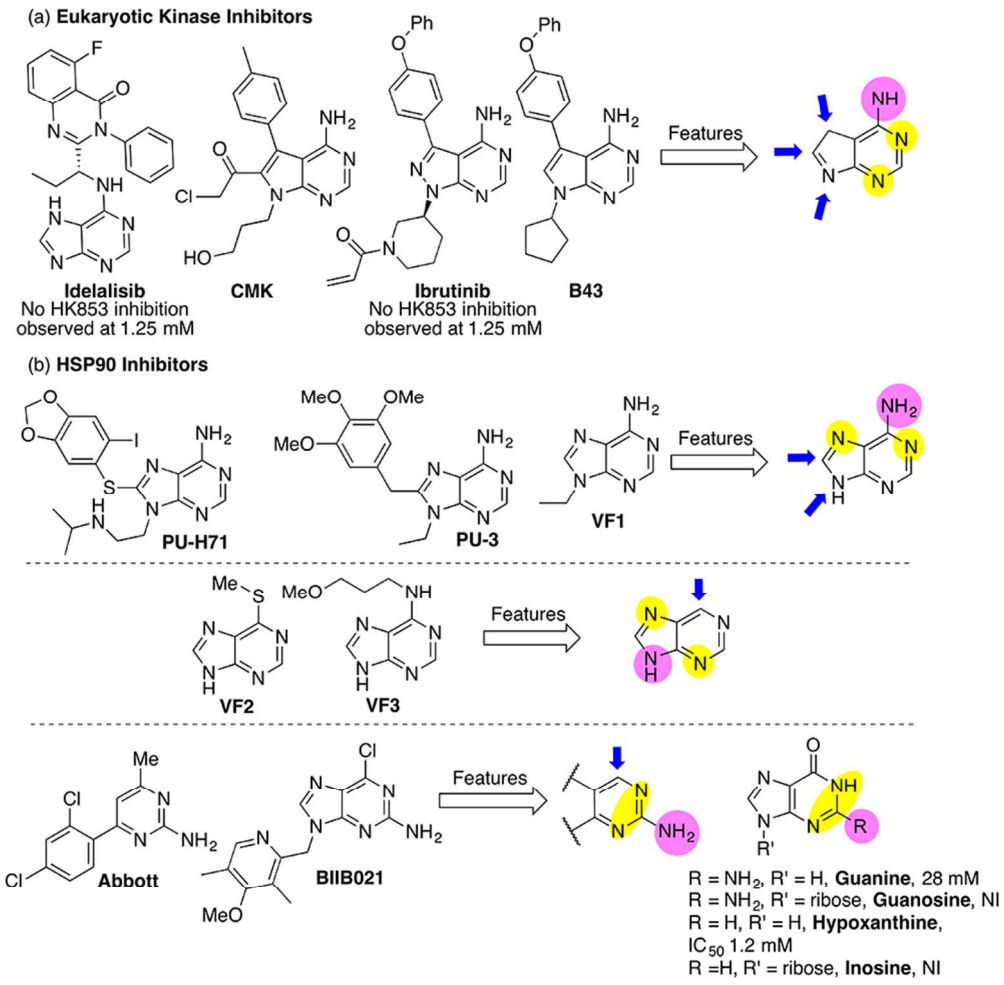

84x82mm (300 x 300 DPI)

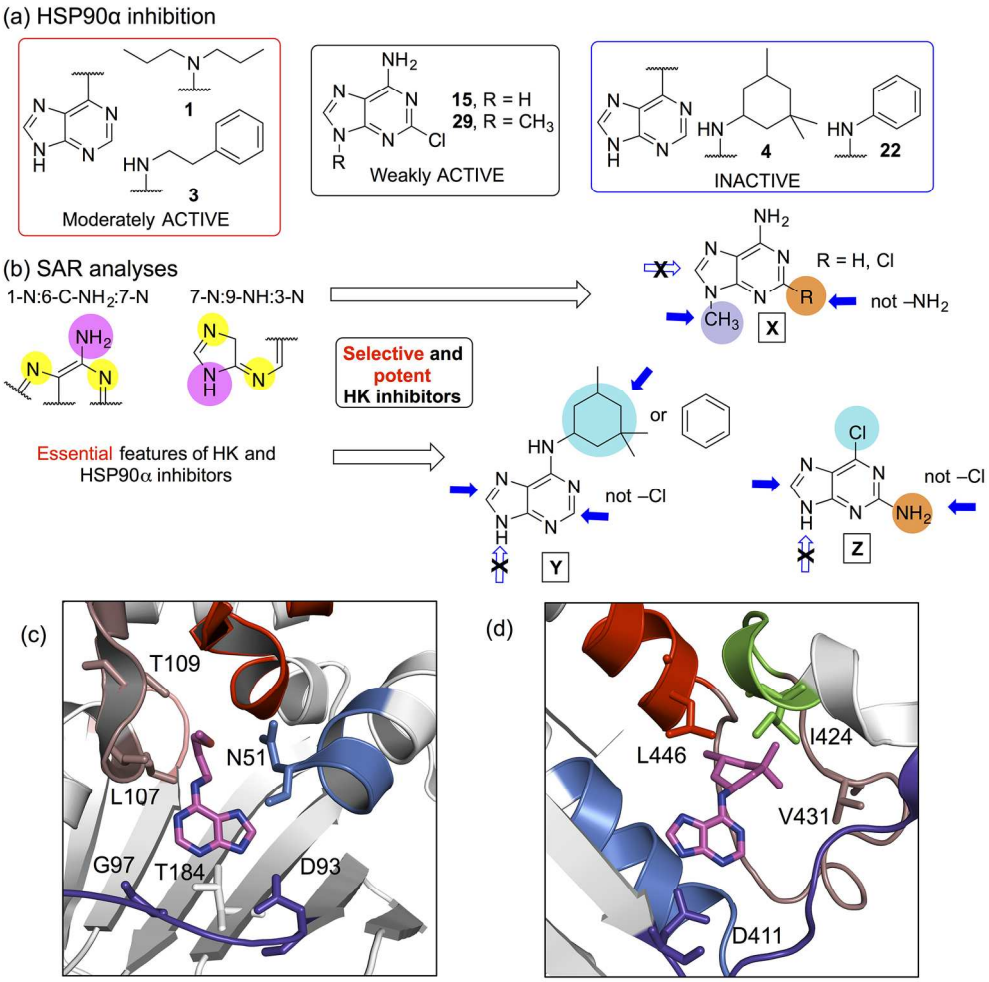

177x177mm (300 x 300 DPI)

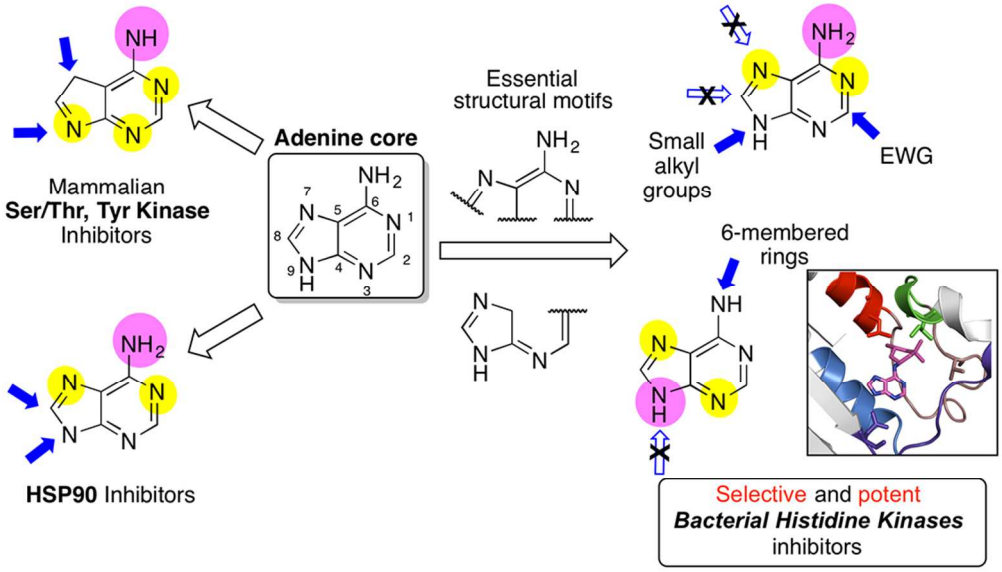

TOC image

96x55mm (300 x 300 DPI)